Volcanic ash leaching as a means of tracing the environmental impact of the 2011 Grímsvötn eruption, Iceland

J. Cabré[1,2], M. Aulinas[2], M. Rejas[1], J.L. Fernandez-Turiel[1]

[1]Institute of Earth Sciences Jaume Almera, ICTJA-CSIC, Lluís Solé i Sabarís s/n, 08028, Barcelona, Spain. e-mail: jlfernandez@ictja.csic.es

[2]Departament de Geoquímica, Petrologia i Prospecció Geològica, Universitat de Barcelona, Martí i Franquès, s/n, 08028, Barcelona, Spain

Abstract

The Grímsvötn volcanic eruption, from 21 to 28 May, 2011, was the largest eruption of the Grímsvötn Volcanic System since 1873, with a Volcanic Explosivity Index (VEI) of magnitude 4. The main geochemical features of the potential environmental impact of the volcanic ash-water interaction were determined using two different leaching methods as proxies (batch and vertical flow-through column experiments). Ash consists of glass with minor amounts of plagioclase, clinopyroxene, diopside, olivine and iron sulfide; this latter mineral phase is very rare in juvenile ash. Ash grain morphology and size reflects the intense interaction of magma and water during eruption. Batch and column leaching tests in deionised water indicate that Na, K, Ca, Mg, Si, Cl, S and F had the highest potential geochemical fluxes to the environment. Release of various elements from volcanic ash took place immediately through dissolution of soluble salts from the ash surface. Element solubilities of Grímsvötn ash

regarding bulk ash composition were <1%. Combining the element solubilities and the total estimated mass of tephra ($7.29x10^{14}$ g), the total input of environmentally important elements were estimated to be $8.91x10^{9}$ g Ca, $7.02x10^{9}$ g S, $1.10x10^{9}$ g Cl, $9.91x10^{8}$ g Mg, $9.91x10^{8}$ g Fe and $1.45x10^{8}$ g P The potential environmental problems were mainly associated with the release of F ($5.19x10^{9}$ g).

Keywords: volcanic ash, water leaching, geochemical flux, Grímsvötn

Introduction

Explosive volcanic eruptions produce mixtures of particulate matter (tephra) and gases that are directly injected into the atmosphere. The interaction of tephra particles with the environment may induce a range of positive and negative physical, chemical and biological effects from local to global scales (Ayris and Delmelle 2012). It is well known that eruptive columns reaching tropospheric and stratospheric heights can have detrimental consequences for the climate, including an increase in greenhouse gases, sulphur and halogen species, as well as aerosols, which could lead to the acidification of precipitation (Robock 2000; Fontijn et al. 2014; Long et al. 2014). On the other hand, volatiles released during an explosive volcanic eruption are usually adsorbed onto the surface of volcanic ash particles as water-soluble compounds (Rose 1977; Ayris and Delmelle 2012). Scavenging of volatiles is variable, with the main elements being sulphur, chlorine and fluorine (Delmelle et al. 2007). After deposition, the adsorbed compounds can be released to the environment where they have the potential to damage water quality, vegetation, livestock and people, although in some cases these effects may be positive, e.g., fertilizing lands and oceans (Wearie and Manly 1996; Duggen et al. 2010; Frogner et al. 2001; Langmann et al. 2010; Witham et al. 2005). An important factor of such compounds is that they dissolve rapidly in contact with water (Olgun et al. 2011; Ayris and Delmelle 2012; Ruggieri et al. 2012a, b).

Other potential human impacts generated by the emission of tephra into the atmosphere include respiratory health hazards for the local population (Horwell and Baxter 2006; Horwell et al. 2013), as well as severe problems for aviation (Casadevall 1994; Guffanti et al. 2009). Recent examples of environmental and

social impacts of volcanic particulate matter are found in the 2010 Eyjafjallajökull and 2011 Grímsvötn (Iceland) eruptions. Both generated a low impact globally, although they caused great disruption to air traffic across Europe, especially the 2010 Eyjafjallajökull eruption (Webster et al. 2012; Witham et al. 2012), and direct effects in Iceland as a result of the ash fall, such as physical damage to roads and bridges, impact on health and loss of crops (Horwell et al. 2013).

The aim of this work is to assess the main geochemical features of the environmental impact of volcanic ash-water interaction using the results of different leaching methods as proxies, through an analysis of the May 2011 Grímsvötn eruption. This work complements the findings of previous studies on this recent volcanic eruption (Oskarsson and Sverrisdóttir 2011; Horwell et al. 2013; Olsson et al. 2013; Sigmarsson et al. 2013), through the analysis of a distinct set of samples and the use of distinct leaching methodologies from previous works on the same eruption, allowing to determine more accurately the potential geochemical fluxes associated with the interaction of volcanic ash with water.

Geological setting

The active Grímsvötn volcanic system (GVS) is aligned along a NE-SW fissure system in south-central Iceland which lies partly beneath the vast Vatnajökull icecap (Fig. 1). Grímsvötn central volcano is located above the Iceland mantle plume, and thus has the highest rate of magma supply along the GVS. Laki fissure is located within the ice-free section of the GVS; in 1783-1784 it produced the largest historic lava flow on Earth, erupting about 14.7 km^3 of lava

and ejecting 0.4 km^3 of dense-rock equivalent volume (V_{DRE}) of tephra (Thordarson and Self 2003). The most recent events in the GVS are the 1996 Gjálp subglacial fissure eruption (Gudmundsson et al. 1997), and the smaller eruptions of 1998 (Sturkell et al. 2003) and 2004 (Jude-Eton et al. 2012). During an eruption, the extensive geothermal activity beneath the Vatnajökull icecap and the subglacial lake bound to the main caldera (Agustsdottir and Brantley 1994; Alfaro et al. 2007) can enhance magma-water interactions (phreatomagmatic eruption) generating a tephra-laden plume that can rise rapidly to the upper troposphere.

The Grímsvötn eruption, which started approximately at 17:30 UTC on 21 May, 2011, was accompanied by an earthquake swarm. The highest eruptive intensity was recorded a few hours after the onset of the eruption when the plume reached a maximum altitude of 20-25 km (Petersen et al. 2012; Hreinsdottir et al. 2014). After 24 hours the ash plume had reached about 100 km to the SW, affecting the villages of Kirkjubærklaustur and Vík (Fig. 1). Visibility in this area during the first few hours was extremely poor. In the following days, winds spread the ash plume over Iceland and distal fallout was even observed in the British Isles, Scandinavia (Kerminen et al. 2011; Tesche et al. 2012), and Baltic countries (Kvietkus et al. 2013). After the first 24 hours of the eruption, the volcanic plume decreased gradually, reaching heights closer to 10 km. On 23 May the height of the plume decreased to 5 km, and on 28 May the volcanic tremors rapidly decreased and finally disappeared at 07:00 UTC (Hreinsdottir et al. 2014). The 21-28 May 2011 eruption was Grímsvötn's largest since 1873, with a Volcanic Explosivity Index (VEI) of magnitude 4 (Hreinsdottir et al. 2014), thus representing a high potential risk through releasing various

elements into water, specially fluorine, which can cause diseases in both animals and humans. Although this volcanic event caused some disruption to European airspace, it was minor compared to the 2010 Eyjafjallajökull eruption.

Methods

Fieldwork was conducted across affected regions of southwestern Iceland on 22 and 25 May, 2011. Most of the ash was released from Grímsvötn before 23 May (Petersen et al. 2012; Olsson et al. 2013), thus sample ISG-0 (Table 1), collected on 22 May at 14:02 UTC, might not contain volcanic ash from the paroxysmal phases of the eruption. The rest of the samples (eight) were collected on 25 May, from 14:32 to 18:27 UTC. It should be noted that sometimes it was slightly rainy during sampling on 25 May. Accordingly, the sampled ash from this day probably underwent some interaction with water, and therefore we classify these samples as fresh rather than pristine. Sampling was carried out along a 100 km transect across the dispersal axis, following the main road through southern Iceland (Fig. 1). This work thus focuses on the effects of the eruption over the downwind region. The ash samples were collected at five sites located at different distances from the vent using a stainless steel shovel (Table 1 and Figs. 1 and 2). Once collected, they were placed in polyethylene bags and transported to the laboratory in which they were dried at 40 °C for 24 hours in an oven and stored in polyethylene vessels until analysis.

Particle size distribution was obtained by laser diffractometry. Morphology and chemistry of ash particles were studied by scanning electron microscope (SEM). Mineralogy was determined by X-ray diffraction (XRD). Concentrations

of major and trace elements in bulk ash samples and leachates were determined by high resolution-inductively coupled plasma-mass spectrometry (HR-ICP-MS). Additional information on analytical methods is provided in the supplementary material.

The volcanic ash leaching experiments were carried out using two independent methods, including a series of batch leaching tests and a flow-through column leaching test. In the batch experiments, 1 g of each ash sample was mixed with 10 ml of Milli-Q Plus ultrapure water type (18.2 MΩ/cm) in 14x100 mm polypropylene test tubes (Ruggieri et al. 2012a and 2012b). Deionised water was chosen as the leachant because it allows a rapid screening of the potentially hazardous species leached from the ash (Witham et al. 2005) and the results are more reliable simulating the leaching by rainwater and are independent of the local surface and groundwater chemistry. The water leachates were shaken at 20 rpm for 4 h and subsequently filtered through polyvinylidene difluoride (PVDF) syringe filters with tube tips (Whatmann, 25 mm diameter and 0.45 μm pore size). Finally, 1% (v/v) HNO_3 was added to bring the volume up to 100 ml. The pH and the specific conductivity (SC) of batch leachates were monitored by means of specific electrodes (Crison Multimeter MM40) immediately after mixing the ash and the deionised water (pH_0 and SC_0), and after shaking (pH_f and SC_f), prior to filtering. The methods used to determine major and trace elements by HR-ICP-MS analysis were based on a previous study (Fernandez-Turiel et al. 2000). Sulphur concentrations are expressed as SO_4^{-2} in the leachates. Fluoride concentrations were determined in the batch leachates prior to filtering using an ion selective electrode (ISE) for fluoride (Orion, Thermo Scientific).

For the flow-through column leaching test, an 8 cm-long and 2.25 cm^2 cross-sectional-area vertical column (Teledyne ISCO Ref. 69-3873-140) was filled with 10 g of the representative ISG-3 ash, as in previous studies (Ruggieri et al. 2012a). Column loading was carried out gradually, allowing the water to percolate through the ash but avoiding the development of air bubbles. A silica filter with an average pore size diameter of 60 Å was attached at the column inlet and outlet. A peristaltic pump (Miniplus 3, Gilson) at the head of the column ensured a constant and stable deionised flow of water (Milli-Q Plus type, 18.2 MΩ/cm) from top to bottom at an average discharge of 0.12 ml/min with ash-water contact time of around 150 minutes. A fraction collector (FC 204, Gilson) at the column outlet directed samples from the leaching solution into 14x100 mm polypropylene test tubes. We employed the drop mode collection, counting 400 drops per tube of aqueous solution from the column outlet. One litre of percolated solution was collected in 6 days, resulting in a set of 100 tube samples. A subset of 37 samples was analysed for major and trace elements by HR-ICP-MS, based on a previous study (Fernandez-Turiel et al. 2000) using acidified (1% HNO_3) dilutions of 1:10 ml, v/v, with Milli-Q Plus type deionised water. Another subset of 39 samples was analysed for pH and SC (Crison Multimeter MM40) immediately after tube filling. Samples were stored at 4 °C until analysis.

Results and discussion

A total of nine samples were collected along the main plume dispersion axis. The ash fall deposited a practically continuous grey to dark grey blanket up to ~100 km to the SW of the Grímsvötn vent in Iceland. A maximum thickness of 30 cm was observed 75 km from the vent in the Skaftá riverbank near

149 Kirkjubæjarklaustur (sampling site ISG-3, Fig. 2). The closest ash fall deposits
150 to the eruptive focus showed two beds separated by a planar boundary. The
151 lower bed had planar lamination (Fig. 2a). Sample ISG-7 was collected from
152 the thicker ash layer (10 cm) in the lower section of the tephra deposit, whereas
153 ISG-8 was collected from the thinner ash layer (0.5 cm) in the upper section
154 (Fig. 2a). Samples ISG-5 (top) and ISG-6 (bottom) were collected a few meters
155 from the previous outcrop where this two-layer structure was less clear. The rest
156 of the samples were collected from deposits with no evidence of bedding or
157 lamination (Figs. 2b-2d).

158 The composition of the 2011 Grímsvötn ash ranged from basaltic to basaltic
159 andesite, with silica content ranging from 50.94 to 56.14 %, m/m (Table 1). The
160 samples are fairly homogeneous in terms of major oxide composition (Table 1),
161 with a broader compositional range for the trace elements. The highest variation
162 coefficients (20-50 %) were shown by V, Cr, As and W.

163 The particle size distribution of the volcanic ash deposits allows two main
164 groups of samples to be distinguished (Fig. 3). The first group consists of
165 unimodal and bimodal size distribution samples, although the dominant modes
166 of the latter group are similar to those of the unimodal size distribution. The size
167 distributions of ash with a maximum of between 72 and 125 μm show that the
168 finer modes are in the more distal outcrops. The second group contains a
169 bimodal distribution, with the dominant mode (753 μm) being coarser than that
170 observed in the previous group (ISG-8) (Fig. 3b). The difference in particle size
171 distribution might be related to variations in fragmentation associated with
172 fluctuations in the volume of water interacting with magma; the ash is finer when
173 the water content increases (Liu et al. 2015). Thus, water might have played a

174 lesser role during the last eruptive period, causing the magma to fragment into
175 coarser ash (sample ISG-8). The origin of the polymodal distribution of ISG-5 is
176 not clear, but could be related to plume transport or wind reworking. Another
177 application for particle size analysis of volcanic ash is the assessment of
178 potential breathing hazards. 'Thoracic' or PM_{10} (<10 μm) particles are likely to
179 cause respiratory diseases and 'respirable' or PM_4 (<4 μm) particles can have
180 the greatest toxic potential (Horwell and Baxter 2006). The particle size analysis
181 of the Grímsvötn ash showed ≤2.7 vol % for <4 μm and ≤6.0 vol % for 10 μm,
182 which is consistent with the previous studies performed with different ash
183 samples from the same eruption (<3.5 vol % <4 μm and <8.4 vol % <10 μm)
184 (Horwell et al. 2013). In comparison, in the 2010 Eyjafjallajökull eruption has
185 been found higher percentages of 'thoracic' and 'respirable' particles (2-13 vol
186 % for <4 μm and 4-26 vol % for <10 μm), varying with the eruptive phase
187 (Horwell et al. 2013). Taking into account the population density of southern
188 Iceland (<3 inhabitants/km^2) (EEA 2010) and the exposure time (8 days), the
189 respiratory health risk of the Grímsvötn ash was low during the eruption and
190 lower still than for the 2010 Eyjafjallajökull eruption.

191 Based on SEM and XRD analyses, the 2011 Grímsvötn ash has >90 % juvenile
192 glass particles. The glass is associated with plagioclase, clinopyroxene,
193 diopside and olivine phenocrysts. This mineralogical composition is coherent
194 with data from previous studies on the erupted 2011 Grímsvötn ash (Olsson et
195 al. 2013; Sigmarsson et al. 2013). An iron sulfide was also present as a minor
196 phase (stoichiometric calculations were made assuming pyrite as the mineral
197 phase observed), which was detected in the XRD measurements for the sample
198 ISG-4. Although some rare occurrences of sulphide globules were indicated

previously in Grímsvötn 2011 ash (Sigmarsson et al. 2013), the presence of iron sulfides, which are highly soluble in water, are presented for first time in this study.

General and detailed SEM images show that blocky shards are very angular and poorly to nonvesicular with curviplanar breakage surfaces (Figs. 4a-b). More rarely, fluidal particles with elongate vesicles (Fig. 4b) and spherical shapes (Fig. 4c) were found. Minor phases such as plagioclase, clinopyroxene, diopside and olivine are difficult to identify using the SEM because glass usually surrounds these crystals. Instead, iron sulfide formed subspherical aggregates of subhedral cubic crystals, partially covered by or free of glass (Fig. 4d). The origin of this iron sulfide is probably the same as that proposed for the sulphide globules, i.e., generated by basalt-sulphide melt exsolution before degassing of the magma (Sigmarsson et al. 2013). The rim textures vary, probably related to differences in cooling rates.

The observed ensemble of shard morphologies is due to the explosive interaction of magma with water that favoured the particle fragmentation. Ash particle aggregates are scarce and could be associated with processes of early ash aggregation in the plume (Bonadonna et al. 2011; Taddeucci et al. 2011). This feature is expressed as bimodality in the particle size distribution of some samples (Fig. 3). However, due to the high water content and the height of the eruption column, more aggregates were expected to be found (Brown et al. 2012). This scarcity of aggregates could be related to the break-up of aggregate during ash fall, as in the 2010 Eyjafjallajökull eruption (Taddeucci et al. 2011).

222 We tried to obtain some proxies for the chemical processes occurring during the
223 interaction of ash and water by means of the batch leaching experiments. This
224 is a simple and fast way to establish the leaching rates of the elements during
225 this interaction. A key question at this point is the ‘pristineness’ of the volcanic
226 ash. Ash samples collected after or during rainfall are different to ash collected
227 under dry conditions due to mobilization of different salts from ash at different
228 rates during the initial ash-water interaction (Taylor and Lichte 1980; Jones and
229 Gislason 2008; Ruggieri et al. 2012a). Accordingly, leachate data might be
230 compromised by rainfall in samples ISG-1 to ISG-8, leading to our classification
231 of them as fresh rather than pristine. In consequence, the results presented in
232 this work must not be taken as ‘absolute’ fluxes of the eruption; however, they
233 fingerprint the 2011 Grímsvötn eruption and indicate the order of magnitude of
234 the fluxes involved.

235 Results of the single batch leaching tests showed a water-leach solution which
236 was slightly acidic immediately after the ash-water interaction, with the
237 exception of three samples which were weakly alkaline, ranging from pH 5.80 to
238 7.62 (Table 2). After shaking for 4 hours, the average pH of leachates increased
239 by around 1.90 pH units, resulting in solutions whose pH ranged between 7.33
240 and 9.26. This increase can be explained by ionic exchange, i.e., dissolution of
241 surface cations and protons of glass and minerals (Gislason and Oelkers 2003;
242 Ruggieri et al. 2010). The behaviour of the explosive ash from Eyjafjallajökull in
243 2010 was similar, with a slightly more basic pH (pH~8) which rose after the ash-
244 water mixing (Gislason et al. 2011). The initial values of specific conductivity
245 (SC) ranged from 7-356 µS/cm (Gislason et al. 2011), increasing in all samples
246 in the final solutions to a range of 14-404 µS/cm (Table 2). The samples with

247 lower values of pH and SC were ISG-5 and ISG-8, the coarser samples and
248 probably more affected by rain (Table 2 and Fig. 3).

249 When the batch results of this work are compared with data from other tephra-
250 leachate studies (Ayris and Delmelle 2012), the Grímsvötn leaching results are
251 at the lower end of the ranges, with clearly lower means and medians, even
252 taking into account the rain effect and the differences in leaching
253 methodologies. The Grímsvötn leaching results are in agreement with the
254 observations in previous works (Ruggieri et al. 2012b; Witham et al. 2012;
255 Olsson et al. 2013).

256 Table 3 compares the batch leached fraction of a Grímsvötn ash (sample ISG-3)
257 with Chaitén 2008 eruption (Chile) and Eyjafjallajökull 2010 eruption (Iceland).
258 The 2008 Chaitén eruption (Ruggieri et al. 2012a) was rhyolitic in composition
259 and is located in a different geological setting, but the batch test was carried out
260 following the same methodology as the one used for the 2011 Grímsvötn ash. In
261 contrast, the 2010 Eyjafjallajökull eruption was compositionally closer to
262 Grímsvötn, and both were located in the same geotectonic setting. However,
263 these samples of the Phase I eruption were not pristine and the solute/ash ratio
264 (1:25), agitation type and time (2 h) used in the batch test were different
265 (Bagnato et al. 2013).

266 Despite the differences, their leached fractions produce similar results in terms
267 of order of magnitude for major elements. The exceptions are Cl and K, which
268 are exceptionally low in the Grímsvötn ash. The remarkably low release of Cl
269 was also found in column leachates (Olsson et al. 2013). Overall, minor and

trace elements are leached at lower rates in the Grímsvötn than in the Chaitén and Eyjafjallajökull ashes.

A proxy for the mobility of elements during the ash-water interaction is the relative mass leached (RML) which is defined as the percentage of the element that can be mobilised through ash-water interaction, and it is expressed as the fraction of the leached element obtained from the batch experiment ($Conc_{batch}$) over the element's bulk concentration ($Conc_{bulk}$). Therefore, RML is expressed as RML % = $Conc_{batch}$ / $Conc_{bulk}$ * 100 (Table 3).

To determine the leached mass for each element, we need to know the total mass of tephra erupted in 2011 by Grímsvötn volcano, which can be estimated using the dense-rock equivalent volume (V_{DRE}) and the density (ρ_{DRE}). The V_{DRE} expresses the volume without the void spaces in the ash particles (vesicles) and the inter-particle space. The V_{DRE} was estimated as being 0.27±0.07 km^3 for this eruption (Hreinsdottir et al. 2014). Assuming a ρ_{DRE} of 2700 kg/m^3, the resulting mass is $7.29x10^{14}$ g. The results obtained for the studied elements are in Table 3.

Each element was classified arbitrarily according to their RML mobility proxy, differentiating between elements with moderate (RML 0.5 to 1.00 %; Sn), low (0.01 to 0.5 %; As, Bi, W, Pb, Sb, Tl, Li, Mo, Zn, Na, Cu, K, Cs, Ca, Sr, Ni, P, Be, Rb, Tb and Ta) and very low mobility (RML<0.01 %; Ge, Rare Earth Elements or REE, Th, Y, Ba, Mg, Mn, Ga, Al, Hf, V, Cr, Co, Fe, Nb, Sc, U, Zr, Ti, Si and Ag). The results show a small degree of mobility for all elements, and remarkably low for major elements. Although the concentrations of Cl, S, B, F, Se, Br, Cd, I and Hg were analysed in the batch experiments, their RML could

not be estimated since their bulk compositions were not determined. Despite the low mobility of elements, the overall quantity released into water may be sizeable (Table 3) by combining the element solubilities and the total estimated mass of tephra. Grímsvötn ash contains notable contents of potential macronutrients ($8.91x10^9$ g Ca, $7.02x10^9$ g S, $9.91x10^8$ g Mg and $1.45x10^8$ g P) and micronutrients ($1.10x10^9$ g Cl and $9.91x10^8$ g Fe) for biological processes, which show the fertilising potential of the ash both in terrestrial ecosystems (Wearie and Manly 1996) and in the surface water of oceans (Duggen et al. 2010; Olgun et al. 2013). Although these values give an estimation of the impacts on marine environment, a leachate study using natural seawater would determine more precisely the impact of the Grímsvötn ash in oceanic waters. Potential environmental problems arising from ash fallout on land or into fresh water systems, on the other hand, are mainly associated with the release of fluoride ($5.19x10^9$ g F), with the hazard of other potentially toxic elements or compounds being extremely low in comparison. It can be observed when contrasting the potential leachable mass of the 2010 Eyjafjallajökull (Bagnato et al. 2013; Gudmundsson et al. 2012) with the 2011 Grímsvötn eruption, that the potential release of macronutrients ($4.79x10^{10}$ g Ca, $1.48x10^{10}$ g S, $2.63x10^9$ g Mg) and Cl ($5.57x10^{10}$ g) to the environment for the former ash was higher, except for Fe ($3.65x10^8$). The potential leachable mass of fluoride in the 2010 eruption was also higher ($1.53x10^{10}$ g) in the Eyjafjallajökull ash. The sulphur fluxes of the 2011 Grímsvötn eruption have been studied previously (Sigmarsson et al. 2013). These authors estimate that $7.3x10^{11}$ g of S were emitted during this eruption, which can be broken down to $7.2x10^{11}$ g of S as SO_2 gas detected by satellite (26 %), $1.2x10^{11}$ g of leachable S (16 %),

319 $3.7x10^{10}$ g of S released in the jöhulhlaups (5 %), and $3.8x10^{11}$ g of S in
320 sulphide globules (53 %). The value obtained for the leachable S content was
321 taken from previous estimations (Olsson et al. 2013). The leachable S value is
322 notably lower in the present work, independent of the leaching method,
323 probably due to prior leaching during rainfall. The results from both previous
324 work and this study on sulphide estimates are equivalent to ~0.3 % of pyrite,
325 which is coherent with our observations by XRD and SEM.

326 The flow-through column leaching test allows the evolution of the leached
327 composition over time to be modelled. The test was carried out with sample
328 ISG-3 due to its representativeness within the 2011 Grímsvötn eruption ash
329 collection. Its selection was done following field and laboratory criteria. Firstly, it
330 was one of the samples not visually affected by rain during sampling, and
331 secondly it is the sample with the most representative particle size distribution.
332 The results are given in Table S1 (supplementary material) and Fig. 5, where
333 they are plotted as progression curves of pH, major and trace elements versus
334 accumulated volume of the percolated solution (Fig. 5).

335 The pH ranges from 6.55 to 7.10, increasing rapidly at the very beginning of the
336 experiment. This trend has been commonly reported in other volcanic ash
337 column leaching tests (Rango et al. 2010; Ruggieri et al. 2010). Once pH has
338 reached its maximum (7.10), the general trend is towards a progressive
339 decrease for about 0.3 units from the beginning to the end, following a saw-
340 tooth pattern. The initial rise in pH was also recognized in the batch experiment
341 and it is likely due to the virtually instantaneous exchange of the alkaline ion by
342 H^+ (or as (H_3O^+), i.e., increase in pH (Ruggieri et al. 2010).The concentrations
343 of the elements in the percolated solution tend to decrease gradually through

time. The high incipient concentrations of SO_4^{2-}, Na, Ca, Mg, K and Sr (Fig. 5) confirm the presence of soluble compounds on ash particle surfaces, originating from interaction between tephra and volcanic gases within the eruption column (Rose 1977; Delmelle et al. 2007). A considerable number of elements show a major peak in concentration between 50 and 60 ml of percolated solution, which sometimes exceeds the initial concentrations (Si, Al, P, Ti, V, Fe, Ni, Cu, Zn, Zr and Ba). This anomaly in the decreasing trend may be due to the incongruent dissolution of volcanic glass by cation-exchange processes (Rango et al. 2010; Ruggieri et al. 2010). Towards the end, the element concentrations become stable, suggesting that the most leachable fraction is exhausted. This situation is reached at relatively small percolated volumes for Na, Si and Cl (~150 ml), indicating a very fast release of these elements, while the stabilization of element concentration for Ti, Mn and Zn is notably higher, by up to 4 times (~600 ml), indicating a more prolonged release over time.

When the discrete column leaching results are plotted on the Chadha diagram (Chadha 1999) for identification of hydrochemical processes, the values group into three sets based on the evolution of the leachate composition (Fig. 6). Set 1 is made up of a single solution that corresponds to the onset of the experiment. Set 2 shows a significant decrease in anion content (Cl^- and SO_4^{2-}) in the solution, whereas set 3 is characterized by a notable reduction in Na, K, Ca and Mg contents, reaching a generally stable situation where no more significant changes are observed (Fig. 6). The batch results are close to the starting value of the column experiment in Fig. 6, with the exception of samples ISG-5 and ISG-8, which also show anomalous behaviour here. This behaviour is interpreted as being partially related to their exposure to rain, and thus the plot

of leaching results on a Chadha diagram could be a useful tool for distinguishing non pristine ash samples. In addition, these two samples belong to the coarser group of samples, pointing out that the anomalous behaviour observed in the Chadha plot could be also related with the fact that finer ash present a larger surface/volume ratio promoting the conditions for the formation of soluble salts on ash surface.

The element masses released in the column experiment are lower than in the batch tests (Table 3). These masses were estimated by interpolating values between analysed samples to complete the data for the total percolated volume. Variations between elements are due to the different physicochemical conditions during the experiments. For the major elements, Si has the closest values for the two methods (8.60×10^8 g in batch vs. 8.17×10^8 g in column). On the other hand, S and Cl have the largest differences (7.02×10^9 vs. 9.73×10^8 g for S and 1.09×10^9 vs. 1.40×10^8 g for Cl, for batch and column tests, respectively). Assuming that batch results reflect the maximum available elemental content of an ash, the column results corroborate their fast release into the environment for practically all the studied elements when ash interacts with water.

Conclusions

The study of the ash generated during the May 2011 eruption of the Icelandic volcano Grímsvötn demonstrates the complementary nature of batch and column leaching experiments in the assessment of the environmental consequences of ejection of ash into the atmosphere and its later deposition on terrestrial and aqueous surfaces. Furthermore, it helps consolidate the

393 methodology for the environmental study of volcanic ash, while at the same
394 time providing new tools to distinguish pristine from non pristine samples.

395 In this scenario, the main findings regarding the May 2011 eruption of
396 Grímsvötn volcano reveal that Na, K, Ca, Mg, Si, Cl, S and F show the largest
397 geochemical fluxes caused by the interaction of water and ash. Additionally, the
398 significant amounts of some of these elements (Ca, S and Mg) together with P,
399 Cl, Fe, which are usually considered as macro/micronutrients, demonstrates the
400 fertilising potential of the May 2011 emitted ash. On the other hand, release of F
401 highlights the possible environmental problems arising from ash fallout on land
402 or into fresh water systems. It is noteworthy that the chemical release is
403 maximal during the first few hours of contact between tephra and water due to
404 the dissolution of soluble salts from the ash surface. As time progresses, these
405 constituents are exhausted, the release drops considerably and elements are
406 freed instead by the incongruent dissolution of the volcanic glass. In addition,
407 the scarce presence of iron sulphide, which is very rare in juvenile ash,
408 underlines the singularity of this sample collection.

409 **Acknowledgments**

410 We gratefully acknowledge the assistance of ICTJA-CSIC labGEOTOP
411 (infrastructure co-funded by ERDF-EU Ref. CSIC08-4E-001) and DRX
412 (infrastructure co-funded by ERDF-EU Ref. CSIC10-4E-141) Surveys (J.
413 Ibañez, J. Elvira and S. Alvarez) and the CCiTUB (SEM Unit) in the analytical
414 work. Financial support was provided by the QUECA Project (MINECO,
415 CGL2011-23307). We appreciate the invaluable comments of Dr. N. Olgun on a
416 previous version of the manuscript. This study was carried out in the framework

of the Research Consolidated Groups GEOPAM (Generalitat de Catalunya, 2014 SGR 869) and GEOVOL, and the Associated Unit CSIC-UB UAGEPE (UA 285P01). We thank Prof. D. Gimeno for the collaboration in different aspects of this work. F. van Wyk de Vries is gratefully acknowledged for useful comments and improvement in English style. Field pictures were taken by Ó. Pérez.

References

Agustsdottir AM, Brantley SL (1994) Volatile fluxes integrated over 4 decades at Grimsvotn volcano, Iceland Journal of Geophysical Research-Solid Earth 99:9505-9522 doi:10.1029/93jb03597

Alfaro R, Brandsdottir B, Rowlands DP, White RS, Gudmundsson MT (2007) Structure of the Grimsvotn central volcano under the Vatnajokull icecap, Iceland Geophysical Journal International 168:863-876 doi:10.1111/j.1365-246X.2006.03238.x

Ayris PM, Delmelle P (2012) The immediate environmental effects of tephra emission Bull Volcanol 74:1905-1936 doi:10.1007/s00445-012-0654-5

Bagnato E et al. (2013) Scavenging of sulphur, halogens and trace metals by volcanic ash: The 2010 Eyjafjallajokull eruption Geochimica Et Cosmochimica Acta 103:138-160 doi:10.1016/j.gca.2012.10.048

Bonadonna C et al. (2011) Tephra sedimentation during the 2010 Eyjafjallajokull eruption (Iceland) from deposit, radar, and satellite observations Journal of Geophysical Research-Solid Earth 116 doi:10.1029/2011jb008462

Brown RJ, Bonadonna C, Durant AJ (2012) A review of volcanic ash aggregation Physics and Chemistry of the Earth 45-46:65-78 doi:10.1016/j.pce.2011.11.001

Casadevall TJ (1994) Volcanic ash and aviation safety; proceedings of the First international symposium on Volcanic ash and aviation safety. USGS Bulletin, vol 2047.

Chadha DK (1999) A proposed new diagram for geochemical classification of natural waters and interpretation of chemical data Hydrogeology Journal 7:431-439 doi:10.1007/s100400050216

Delmelle P, Lambert M, Dufrene Y, Gerin P, Oskarsson N (2007) Gas/aerosol-ash interaction in volcanic plumes: New insights from surface analyses of fine ash particles Earth and Planetary Science Letters 259:159-170 doi:10.1016/j.epsl.2007.04.052

Duggen S, Olgun N, Croot P, Hoffmann L, Dietze H, Delmelle P, Teschner C (2010) The role of airborne volcanic ash for the surface ocean biogeochemical iron-cycle: a review Biogeosciences 7:827-844 doi:10.5194/bg-7-827-2010

EEA (2010) The European environment - state and outlook 2010: synthesis. Country assessments. Iceland. Population density. European Environment Agency, Copenhagen

Fernandez-Turiel JL, Llorens JF, Lopez-Vera F, Gomez-Artola C, Morell I, Gimeno D (2000) Strategy for water analysis using ICP-MS Fresenius Journal of Analytical Chemistry 368:601-606

Fontijn K, Lachowycz SM, Rawson H, Pyle DM, Mather TA, Naranjo JA, Moreno-Roa H (2014) Late Quaternary tephrostratigraphy of southern Chile and Argentina Quaternary Science Reviews 89:70-84 doi:10.1016/j.quascirev.2014.02.007

462 Frogner P, Gislason SR, Oskarsson N (2001) Fertilizing potential of volcanic ash in
463 ocean surface water Geology 29:487-490
464 Gislason SR et al. (2011) Characterization of Eyjafjallajokull volcanic ash particles and
465 a protocol for rapid risk assessment Proceedings of the National Academy of
466 Sciences of the United States of America 108:7307-7312
467 doi:10.1073/pnas.1015053108
468 Gislason SR, Oelkers EH (2003) Mechanism, rates, and consequences of basaltic
469 glass dissolution: II. An experimental study of the dissolution rates of basaltic
470 glass as a function of pH and temperature Geochimica Et Cosmochimica Acta
471 67:3817-3832 doi:10.1016/s0016-7037(00)00176-5
472 Gudmundsson MT, Sigmundsson F, Bjornsson H (1997) Ice-volcano interaction of the
473 1996 Gjalp subglacial eruption, Vatnajokull, Iceland Nature 389:954-957
474 doi:10.1038/40122
475 Guffanti M, Mayberry GC, Casadevall TJ, Wunderman R (2009) Volcanic hazards to
476 airports Natural Hazards 51:287-302 doi:10.1007/s11069-008-9254-2
477 Horwell CJ, Baxter PJ (2006) The respiratory health hazards of volcanic ash: a review
478 for volcanic risk mitigation Bull Volcanol 69:1-24 doi:10.1007/s00445-006-0052-
479 y
480 Horwell CJ et al. (2013) Physicochemical and toxicological profiling of ash from the
481 2010 and 2011 eruptions of Eyjafjallajokull and Grimsvotn volcanoes, Iceland
482 using a rapid respiratory hazard assessment protocol Environmental Research
483 127:63-73 doi:10.1016/j.envres.2013.08.011
484 Hreinsdottir S et al. (2014) Volcanic plume height correlated with magma-pressure
485 change at Grimsvotn Volcano, Iceland Nature Geoscience 7:214-218
486 doi:10.1038/ngeo2044
487 Icelandic-Meteorological-Office (2010) Grímsvötn 2010. Jökulhlaup - glacier outburst
488 flood in 2010. http://en.vedur.is/hydrology/articles/nr/2040. Accessed
489 04/07/2014
490 Icelandic-Metereological-Office (2011) Web-pages related to the Grímsvötn eruption
491 2011. Vatnajökull monitoring. GPS displacement at Grímsfjall since 2006.
492 http://hraun.vedur.is/ja/vatnajokulsvoktun/gps_faersla.html. Accessed
493 04/07/2014
494 Jones MT, Gislason SR (2008) Rapid releases of metal salts and nutrients following the
495 deposition of volcanic ash into aqueous environments Geochimica Et
496 Cosmochimica Acta 72:3661-3680 doi:10.1016/j.gca.2008.05.030
497 Jude-Eton TC, Thordarson T, Gudmundsson MT, Oddsson B (2012) Dynamics,
498 stratigraphy and proximal dispersal of supraglacial tephra during the ice-
499 confined 2004 eruption at Grimsvotn Volcano, Iceland Bull Volcanol 74:1057-
500 1082 doi:10.1007/s00445-012-0583-3
501 Kerminen VM et al. (2011) Characterization of a volcanic ash episode in southern
502 Finland caused by the Grimsvotn eruption in Iceland in May 2011 Atmospheric
503 Chemistry and Physics 11:12227-12239 doi:10.5194/acp-11-12227-2011
504 Kvietkus K, Sakalys J, Didzbalis J, Garbariene I, Spirkauskaite N, Remeikis V (2013)
505 Atmospheric aerosol episodes over Lithuania after the May 2011 volcano
506 eruption at Grimsvotn, Iceland Atmospheric Research 122:93-101
507 doi:10.1016/j.atmosres.2012.10.014
508 Langmann B, Zaksek K, Hort M, Duggen S (2010) Volcanic ash as fertiliser for the
509 surface ocean Atmospheric Chemistry and Physics 10:3891-3899
510 Liu EJ, Cashman KV, Rust AC, Gislason SR (2015) The role of bubbles in generating
511 fine ash during hydromagmatic eruptions Geology 43(3):239-242
512 Long CJ, Power MJ, Minckley TA, Hass AL (2014) The impact of Mt Mazama tephra
513 deposition on forest vegetation in the Central Cascades, Oregon, USA
514 Holocene 24:503-511 doi:10.1177/0959683613520258
515 Olgun N, Duggen S, Andronico D, Kutterolf S, Croot PL, Giammanco S, Censi P,
516 Randazzo L (2013) Possible impacts of volcanic ash emissions of Mount Etna

517 on the primary productivity in the oligotrophic Mediterranean Sea: Results from
518 nutrient-release experiments in seawater Marine Chemistry 152:32-42
519 doi:10.1016/j.marchem.2013.04.004
520 Olgun N, Duggen S, Croot PL, Delmelle P, Dietze H, Schacht U, Oskarsson N, Siebe
521 C, Auer A, Garbe-Schönberg D (2011) Surface ocean iron fertilization: The role
522 of airbone volcanic ash from subduction zone and hot spot volcanoes and
523 related iron fluxes into Pacific Ocean Global Biogeochemical Cycles 25
524 Olsson J, Stipp SLS, Dalby KN, Gislason SR (2013) Rapid release of metal salts and
525 nutrients from the 2011 Grimsvotn, Iceland volcanic ash Geochimica Et
526 Cosmochimica Acta 123:134-149 doi:10.1016/j.gca.2013.09.009
527 Oskarsson N, Sverrisdottir G (2011) Chemical composition and texture of ash from the
528 Grímsvötn 2011-eruption. Institute of Earth Sciences, University of Iceland,
529 2011, available online at: http://earthice.hi.is/page/ies GV2011 chemical
530 Petersen GN, Bjornsson H, Arason P, von Löwis S (2012) Two weather radar time
531 series of the altitude of the volcanic plume during the May 2011 eruption of
532 Grímsvötn, Iceland Earth Syst Sci Data 4:121-127 doi:10.5194/essd-4-121-
533 2012
534 Rango T, Colombani N, Mastrocicco M, Bianchini G, Beccaluva L (2010) Column
535 Elution Experiments on Volcanic Ash: Geochemical Implications for the Main
536 Ethiopian Rift Waters Water Air and Soil Pollution 208:221-233
537 doi:10.1007/s11270-009-0161-2
538 Robock A (2000) Volcanic eruptions and climate Reviews of Geophysics 38:191-219
539 doi:10.1029/1998rg000054
540 Rose WI (1977) Scavenging of volcanic aerosol by ash - atmospheric and volcanologic
541 implications Geology 5:621-624
542 Ruggieri F et al. (2012a) Contribution of volcanic ashes to the regional geochemical
543 balance: The 2008 eruption of Chaiten volcano, Southern Chile Science of the
544 Total Environment 425:75-88 doi:10.1016/j.scitotenv.2012.03.011
545 Ruggieri F et al. (2012b) Multivariate factorial analysis to design a robust batch
546 leaching test to assess the volcanic ash geochemical hazard Journal of
547 Hazardous Materials 213:273-284 doi:10.1016/j.jhazmat.2012.01.091
548 Ruggieri F, Saavedra J, Fernandez-Turiel JL, Gimeno D, Garcia-Valles M (2010)
549 Environmental geochemistry of ancient volcanic ashes Journal of Hazardous
550 Materials 183:353-365 doi:10.1016/j.jhazmat.2010.07.032
551 Sigmarsson O, Haddadi B, Carn S, Moune S, Gudnason J, Yang K, Clarisse L (2013)
552 The sulfur budget of the 2011 Grimsvotn eruption, Iceland Geophysical
553 Research Letters 40:6095-6100 doi:10.1002/2013gl057760
554 Sturkell E, Einarsson L, Sigmundsson F, Hreinsdottir S, Geirsson H (2003) Deformation
555 of Grimsvotn volcano, Iceland: 1998 eruption and subsequent inflation
556 Geophysical Research Letters 30 doi:10.1029/2002gl016460
557 Taddeucci J et al. (2011) Aggregation-dominated ash settling from the Eyjafjallajokull
558 volcanic cloud illuminated by field and laboratory high-speed imaging Geology
559 39:891-894 doi:10.1130/g32016.1
560 Taylor HE, Lichte FE (1980) Chemical composition of Mount St-Helens volcanic ash
561 Geophysical Research Letters 7:949-952 doi:10.1029/GL007i011p00949
562 Tesche M et al. (2012) Volcanic ash over Scandinavia originating from the Grimsvotn
563 eruptions in May 2011 Journal of Geophysical Research-Atmospheres 117
564 doi:10.1029/2011jd017090
565 Thordarson T, Self S (2003) Atmospheric and environmental effects of the 1783-1784
566 Laki eruption: A review and reassessment Journal of Geophysical Research-
567 Atmospheres 108 doi:10.1029/2001jd002042
568 Weaire J, Manly R (1996) Chemical quality water studies in the Central Patagonian
569 Region of Chile following the eruption of Volcan Hudson Hydrobiologia
570 331:161-166

571 Webster HN et al. (2012) Operational prediction of ash concentrations in the distal
572 volcanic cloud from the 2010 Eyjafjallajokull eruption Journal of Geophysical
573 Research-Atmospheres 117 doi:10.1029/2011jd016790
574 Witham C, Webster H, Hort M, Jones A, Thomson D (2012) Modelling concentrations of
575 volcanic ash encountered by aircraft in past eruptions Atmospheric Environment
576 48:219-229 doi:10.1016/j.atmosenv.2011.06.073
577 Witham CS, Oppenheimer C, Horwell CJ (2005) Volcanic ash-leachates: a review and
578 recommendations for sampling methods Journal of Volcanology and
579 Geothermal Research 141:299-326 doi:10.1016/j.jvolgeores.2004.11.010

580

581 **Table captions**

582 **Table 1.** Main features of the studied ash from the 2011 Grímsvötn eruption.
583 Mineral compositions: ***, prevalent; **, common; *, frequent; (*), scarce; nd, not
584 detected. Major oxides and loss on ignition (LOI) expressed as %, m/m. Trace
585 elements expressed as µg/g.

586 **Table 2.** pH and specific conductivity (SC) of the batch leaching tests of
587 Grímsvötn samples which were monitored immediately after mixing the ash and
588 the deionised water (pH_0 and SC_0), and after 4 hours shaking (pH_f and SC_f)
589 without filtering. SC is expressed as µS/cm.

590 **Table 3.** Potential geochemical fluxes associated with the 2011 Grímsvötn
591 eruption. Data for batch (1 g volcanic ash was shaken with 10 ml of deionized
592 water for 4 h) and column leaching (10 g ash were leached in a flow-through
593 column with 1000 ml of deionized water pumped at 0.12 ml/min) experiments
594 are shown for the same sample (ISG-3), chosen for its preservation and particle
595 size distribution. Batch results are compared with an average of ash batch tests
596 (Ayris and Delmelle 2012), sample CH-1F of 2008 Chaitén eruption (Ruggieri et
597 al. 2012a), and mean values of samples from the first eruptive phase of the
598 2010 Eyjafjallajökull eruption (Bagnato et al. 2013). nd, not determined; <LoD,
599 lower than limit of detection.

600

601

602 **Figure captions**

603 **Fig. 1.** Map showing the locations of volcanic ash samples, Grímsvötn volcano
604 and other active volcanoes in southern Iceland, icecaps and urban areas.

605 **Fig. 2.** Photographs showing the ash sampling sites located at different
606 distances from Grímsvötn volcano including; a, The most proximal to vent ash
607 fall deposit sampled (49 km), with two beds; the lower shows parallel
608 lamination. b, Massive deposit at site ISG-3, with the maximum thickness
609 observed (30 cm), at 75 km from the vent in the Skaftá riverbank near
610 Kirkjubæjarklaustur; the upper part was slightly hardened. c, Massive deposit on
611 the Brunná riverbank (57 km from the vent). d, Laki lava lightly covered by ash
612 (95 km from the vent).

613 **Fig. 3.** Particle size distribution of Grímsvötn 2011 ash of (a) samples with
614 unimodal distribution, and (b) samples with bimodal and polymodal distribution.

615 **Fig. 4.** SEM images of the studied ash from the 2011 Grímsvötn eruption.
616 Blocky shards are very angular and poorly to nonvesicular with curviplanar
617 breakage surfaces (a, b). More scarcely, we found fluidal particles with elongate
618 vesicles (b) and spherical shapes (c). d An iron sulphide. Images a–c were
619 captured with an EverhartThornley detector (ETD), whereas d was taken with a
620 backscattered electron detector (BSED). a, c ISG3. b ISG6. d ISG4

621 **Fig. 5.** Changes in the element concentrations, pH and SC of the ash-leachate
622 of ISG-3 ash sample from Grímsvötn 2011 eruption during the flow-through
623 column experiment in deionized water. Ten grams of ash were leached in a
624 flow-through column with 1000 ml (percolate volume) of deionized water
625 pumped at 0.12 ml/min with ash-water contact time of around 150 minutes.

626 **Fig. 6.** Chadha diagram (Chadha 1999) of the chemical compositions of the
627 batch (1 g of volcanic ash was shaken with 10 ml of deionized water for 4 h)
628 and column leachates (10 g of ash were leached in a flow-through column with
629 1000 ml of deionized water pumped at 0.12 ml/min). This plot shows the
630 difference between divalent alkaline cations (Ca^{2+} and Mg^{2+}) and monovalent
631 alkaline cations (Na^{+} and K^{+}) in milliequivalent (meq) percentage over the
632 difference between weak (HCO^{3-}) and strong (Cl^{-} and SO_4^{2-}) acid anions. Red
633 numbers correspond to the different steps of the leaching process observed in
634 the column test in sample ISG-3.

635 **Supplementary material**

636 **Supplementary material –** Details on analytical methods and leaching tests.

637 **Supplementary Table S1.** pH, specific conductivity and concentrations of the

638 flow-through column experiment of ISG-3 sample.

Table 1. Main features of the studied ashes from 2011 Grímsvötn eruption. Mineral composition: ***, prevalent; **, common; *, frequent; (*), scarce; nd, not detected. Major oxides and loss on ignition (LOI) expressed as %, m/m. Trace elements expressed as µg/g.

	ISG-0	ISG-1	ISG-2	ISG-3	ISG-4	ISG-5	ISG-6	ISG-7	ISG-8
Latitude	63°47'22"N	63°40'18"N	63°47'38"N	63°47'38"N	63°54'40"N	63°57'23"N	63°57'23"N	63°57'23"N	63°57'23"N
Longitude	18°03'02"W	18°24'13"W	18°02'17"W	18°02'17"W	17°43'14"W	17°26'58"W	17°26'58"W	17°26'58"W	17°26'58"W
Location	Kirkjubæjar-klaustur	Laki lava	Skaftá river (Kirkjubæjar-klaustur)	Skaftá river (Kirkjubæjar-klaustur)	Brunná river	Skeiðarársandur	Skeiðarársandur	Skeiðarársandur	Skeiðarársandur
Distance from the vent (km)	75	95	75	75	57	49	49	49	49
Thickness (cm)	2	0-4	8	30	24	25	10.5	10	0.5
Collection date	22/05/2011	25/05/2011	25/05/2011	25/05/2011	25/05/2011	25/05/2011	25/05/2011	25/05/2011	25/05/2011
Preservation	Pristine	Fresh	Fresh	Fresh	Fresh	Fresh	Fresh	Fresh	Fresh
Glass	***	***	***	***	***	***	***	***	***
Augite	nd	nd	nd	nd	nd	**	nd	nd	**
Anorthite	nd	nd	nd	nd	nd	*	nd	nd	*
Pyrite	nd	nd	nd	nd	(*)	nd	nd	nd	nd
SiO_2	56.14	52.49	52.23	50.94	54.49	52.07	51.40	55.80	55.25
Al_2O_3	12.26	12.78	12.64	13.53	12.73	12.99	14.01	11.88	12.94
Fe_2O_3 total	12.70	13.45	13.50	13.62	13.28	12.60	13.21	12.44	12.19
MnO	0.22	0.23	0.24	0.23	0.24	0.23	0.23	0.22	0.22
MgO	4.99	5.04	5.17	5.22	4.94	5.73	4.99	4.63	5.92
CaO	8.94	9.25	9.29	9.54	9.18	10.13	9.64	8.67	10.53
Na_2O	2.72	2.81	2.99	2.93	2.85	2.70	2.74	2.64	2.55
K_2O	0.47	0.49	0.49	0.50	0.51	0.43	0.47	0.47	0.42
TiO_2	2.61	2.76	2.78	2.82	2.81	2.49	2.64	2.60	2.38
P_2O_5	0.38	0.39	0.38	0.38	0.38	0.32	0.37	0.35	0.29
LOI	-0.87	-0.76	-0.35	-0.36	-0.82	-0.69	-0.94	-1.04	0.12
Total	100.56	98.94	99.35	99.34	100.59	99.01	98.76	98.66	102.82
Li	6.11	6.40	6.38	6.43	6.44	5.60	6.03	5.83	5.57
Be	0.98	0.99	0.97	1.06	1.01	0.85	0.93	0.97	0.78
Sc	36.8	37.8	38.5	39.4	38.1	42.1	39.8	36.2	42.5
V	205	282	206	256	339	213	194	207	330
Cr	37.7	33.6	43.4	28.9	37.3	78.4	52.4	41.9	78.0
Co	36.5	37.5	37.4	38.7	37.8	39.6	37.9	35.7	39.3
Ni	35.9	35.6	37.2	37.7	35.9	47.8	39.7	35.1	53.5
Cu	92.1	92.3	92.3	93.4	91.2	108	96.1	86.8	118
Zn	104	114	101	106	104	111	101	98.3	95.6
Ga	17.6	18.2	17.9	18.0	17.9	18.2	18.1	17.2	17.9
Ge	1.65	1.32	1.65	1.66	1.23	1.79	1.74	1.57	1.46
As	0.24	0.16	0.33	0.36	0.11	0.18	0.21	0.25	0.11
Rb	8.58	8.85	8.89	8.99	8.85	7.60	8.30	8.49	8.27
Sr	195	202	209	216	212	198	205	195	202
Y	37.4	39.6	40.6	41.1	40.8	35.7	38.4	38.0	34.4
Zr	205	212	216	221	219	179	206	210	172
Nb	19.9	20.6	20.0	20.0	20.5	17.1	19.1	18.4	15.5
Mo	0.65	0.60	0.61	0.63	0.63	0.52	0.58	0.61	0.49
Sn	1.14	1.16	1.20	1.20	1.17	1.07	1.10	1.18	1.09
Sb	0.04	0.05	0.04	0.04	0.04	0.04	0.04	0.05	0.04
Cs	0.08	0.09	0.09	0.09	0.09	0.08	0.08	0.09	0.07
Ba	91.3	95.0	97.6	96.2	96.1	82.5	90.1	90.8	83.4
La	14.5	14.7	15.2	15.2	15.4	13.0	14.5	13.8	12.4
Ce	34.2	36.1	36.7	36.0	36.6	31.2	33.8	34.2	29.0
Pr	4.89	5.11	5.07	5.15	5.23	4.32	4.79	4.83	4.18
Nd	22.1	23.4	23.7	24.1	24.1	20.0	22.6	22.3	19.0
Sm	6.06	6.41	6.48	6.69	6.48	5.53	6.14	6.06	5.57
Eu	1.85	1.95	1.96	1.98	1.98	1.74	1.85	1.78	1.70
Gd	6.59	6.98	6.99	7.23	7.21	6.08	6.72	6.62	6.08
Tb	1.04	1.08	1.11	1.14	1.11	0.97	1.05	1.05	0.96
Dy	6.75	6.92	7.12	7.08	7.15	6.21	6.66	6.65	6.20
Ho	1.16	1.21	1.20	1.23	1.24	1.09	1.17	1.13	1.08
Er	3.40	3.60	3.67	3.68	3.72	3.26	3.42	3.40	3.19
Tm	0.57	0.60	0.61	0.62	0.62	0.55	0.58	0.58	0.54
Yb	3.42	3.57	3.68	3.69	3.69	3.21	3.47	3.44	3.18
Lu	0.53	0.55	0.57	0.57	0.56	0.48	0.52	0.52	0.49
Hf	4.08	4.17	4.11	4.12	4.29	3.52	3.99	3.94	3.45
Ta	1.01	1.03	1.00	1.04	1.07	0.85	0.93	0.95	0.82
W	0.22	0.22	0.22	0.22	0.22	0.19	0.21	0.49	0.19
Tl	0.02	0.02	0.02	0.02	0.02	0.02	0.02	0.02	0.02
Pb	1.28	1.25	1.32	1.24	1.21	1.21	1.40	1.14	1.18
Bi	0.01	0.01	0.02	0.01	0.01	0.01	0.01	0.01	0.01
Th	1.22	1.28	1.32	1.31	1.31	1.11	1.20	1.22	1.12
U	0.36	0.39	0.39	0.39	0.40	0.33	0.35	0.36	0.32

Table 2. pH and specific conductivity (SC) of the batch leaching tests of Grímsvötn samples which were monitored immediately after mixing the ash and the deionised water (pH_0 and SC_0), and after 4 hours shaking (pH_f and SC_f) without filtering. SC is expressed as µS/cm.

Parameter	Unit	ISG-0	ISG-1	ISG-2	ISG-3	ISG-4	ISG-5	ISG-6	ISG-7	ISG-8
pH_0	pH unit	7.62	7.20	6.65	6.80	7.20	6.12	6.00	6.10	5.80
pH_f	pH unit	8.93	8.84	7.75	8.22	9.26	7.68	8.17	8.84	7.33
SC_0	µS/cm	90	117	356	101	43	18	86	96	7
SC_f	µS/cm	244	148	404	122	100	28	110	130	15
Ca	mg/l	2.04	1.77	3.62	1.22	1.03	0.64	0.89	1.26	0.42
Mg	mg/l	0.23	0.16	0.54	0.14	0.11	0.10	0.13	0.13	0.06
Na	mg/l	1.39	0.80	2.41	0.71	0.58	0.25	0.70	0.72	0.24
K	mg/l	0.11	0.11	0.13	0.10	0.08	0.11	0.10	0.07	0.11
Si	mg/l	0.18	0.21	0.15	0.12	0.11	0.17	0.11	0.13	0.15
Cl	mg/l	0.29	0.15	0.54	0.15	0.11	0.10	0.13	0.15	0.10
SO_4	mg/l	6.02	3.47	12.80	2.89	2.42	0.63	2.80	3.15	0.34
F	mg/l	1.73	0.90	1.37	0.71	0.81	0.08	0.58	0.88	0.02
Li	µg/l	0.61	0.39	0.81	0.30	0.27	0.11	0.34	0.33	0.11
Be	µg/l	0.01	0.02	0.01	0.01	0.01	0.01	0.01	0.01	0.02
B	µg/l	27.6	26.0	17.2	17.9	19.3	24.3	29.2	17.8	27.2
Al	µg/l	180.7	372.5	188.4	168.1	201.7	264.3	223.6	183.4	272.7
P	µg/l	23.4	35.0	21.1	19.8	18.1	19.2	13.8	19.3	17.6
Sc	µg/l	0.07	0.11	0.06	0.06	0.06	0.08	0.05	0.06	0.06
Ti	µg/l	6.54	19.00	7.52	6.06	8.76	11.93	8.11	8.47	8.49
V	µg/l	0.91	1.50	0.72	0.63	0.71	0.65	0.57	0.80	0.62
Cr	µg/l	0.08	0.12	0.09	0.13	0.10	0.23	0.11	0.07	0.17
Fe	µg/l	173.9	382.9	187.8	135.9	173.6	195.1	138.8	184.6	130.7
Mn	µg/l	11.40	14.69	12.54	10.71	8.43	5.08	6.53	8.65	2.93
Co	µg/l	0.11	0.17	0.07	0.08	0.09	0.07	0.08	0.09	0.05
Ni	µg/l	0.66	0.79	0.52	0.80	0.57	0.39	0.56	0.48	0.72
Cu	µg/l	2.45	6.87	3.64	2.69	3.12	1.95	2.27	3.09	1.61
Zn	µg/l	4.29	5.11	4.94	5.21	3.70	4.00	3.70	3.12	7.07
Ga	µg/l	0.08	0.12	0.06	0.05	0.06	0.05	0.06	0.07	0.04
Ge	µg/l	0.02	0.02	0.02	0.01	0.01	0.02	0.02	0.01	0.01
As	µg/l	0.03	0.10	0.03	0.03	0.07	0.03	0.13	0.04	0.10
Se	µg/l	1.92	2.08	1.10	1.00	0.76	1.31	-0.21	1.33	1.46
Rb	µg/l	0.10	0.12	0.13	0.09	0.08	0.09	0.08	0.08	0.07
Sr	µg/l	4.89	3.85	8.00	2.92	2.33	2.05	2.06	2.90	1.22
Y	µg/l	0.36	0.51	0.33	0.27	0.25	0.35	0.17	0.29	0.23
Zr	µg/l	0.13	0.18	0.13	0.12	0.14	0.13	0.24	0.10	0.20
Nb	µg/l	0.04	0.04	0.04	0.04	0.03	0.04	0.04	0.03	0.04
Mo	µg/l	0.05	0.04	0.06	0.03	0.02	0.02	0.02	0.03	0.02
Ag	µg/l	0.02	0.02	0.02	0.03	0.02	0.02	0.02	0.01	0.02
Cd	µg/l	0.02	0.02	0.02	0.02	0.01	0.01	0.01	0.01	0.01
Sn	µg/l	0.95	0.86	1.05	1.31	0.80	1.10	0.87	0.60	0.96
Sb	µg/l	0.014	0.005	0.007	0.007	0.004	0.005	0.003	0.006	0.009
I	µg/l	0.27	0.29	0.24	0.22	0.19	0.22	0.20	0.18	0.19
Cs	µg/l	0.003	0.002	0.002	0.002	0.002	0.002	0.002	0.002	0.002
Ba	µg/l	0.67	0.67	0.68	0.57	0.45	0.60	0.47	0.44	0.52
La	µg/l	0.160	0.224	0.145	0.117	0.111	0.165	0.081	0.127	0.111
Ce	µg/l	0.387	0.526	0.313	0.274	0.260	0.356	0.185	0.303	0.240
Pr	µg/l	0.054	0.074	0.045	0.039	0.036	0.051	0.025	0.042	0.034
Nd	µg/l	0.253	0.359	0.211	0.174	0.173	0.249	0.122	0.203	0.164
Sm	µg/l	0.062	0.097	0.056	0.049	0.046	0.057	0.030	0.053	0.041
Eu	µg/l	0.022	0.029	0.019	0.014	0.014	0.018	0.010	0.017	0.012
Gd	µg/l	0.076	0.105	0.065	0.050	0.049	0.065	0.032	0.060	0.045
Tb	µg/l	0.014	0.018	0.012	0.010	0.009	0.013	0.007	0.011	0.008
Dy	µg/l	0.078	0.111	0.059	0.053	0.052	0.069	0.032	0.063	0.047
Ho	µg/l	0.014	0.019	0.012	0.010	0.009	0.012	0.006	0.011	0.009
Er	µg/l	0.038	0.055	0.034	0.026	0.026	0.036	0.017	0.031	0.025
Tm	µg/l	0.005	0.007	0.004	0.003	0.003	0.005	0.002	0.004	0.003
Yb	µg/l	0.031	0.041	0.024	0.021	0.020	0.028	0.014	0.024	0.020
Lu	µg/l	0.004	0.006	0.004	0.003	0.003	0.005	0.002	0.003	0.003
Hf	µg/l	0.017	0.017	0.012	0.011	0.011	0.011	0.015	0.011	0.013
Ta	µg/l	0.010	0.012	0.010	0.010	0.009	0.011	0.011	0.007	0.010
W	µg/l	0.06	0.06	0.06	0.12	0.06	0.07	0.06	0.04	0.06
Hg	µg/l	0.022	0.009	0.007	0.008	0.006	0.001	0.006	0.010	0.001
Tl	µg/l	0.003	0.004	0.003	0.003	0.003	0.003	0.003	0.002	0.003
Pb	µg/l	0.22	0.30	0.42	0.35	0.25	0.25	0.29	0.17	0.28
Bi	µg/l	0.004	0.004	0.003	0.003	0.003	0.003	0.003	0.003	0.003
Th	µg/l	0.013	0.013	0.013	0.008	0.008	0.008	0.010	0.009	0.008
U	µg/l	0.003	0.010	0.003	0.004	0.007	0.005	0.011	0.004	0.010

Table 3. Potential geochemical fluxes associated with the 2011 Grímsvötn eruption. Data of batch (1 g of volcanic ash was contacted with 10 ml of deionized water during 4 h) and column leaching (10 g of ash were leached in a flow-through column with 1000 ml of deionized water pumped at 0.12 ml/min) experiments are reported for the same sample (ISG-3), chosen for its representativeness. Batch results are compared with an average of ash batch tests (Ayris and Delmelle, 2012), sample CH-1F of 2008 Chaitén eruption (Ruggieri et al., 2012a), and mean values of samples from the first eruptive phase of 2010 Eyjafjallajökull eruption (Bagnato et al., 2013). nd, not determined; <LoD, lower than limit of detection.

Element	Batch leached fraction average Ayris and Delmelle 2012 mg/kg				Count	Batch leached fraction			Grímsvötn 2011 this work				
						Chaitén 2008 Ruggieri et al. 2012	Eyjafjallajökull 2010 Bagnato et al. 2012	Grímsvötn 2011 this work	Bulk mass	Leachable mass (batch)		Leachable mass (column)	
	Max	Min	Mean	Median		mg/kg	mg/kg	mg/kg	mt	mt	% of bulk (RML)	mt	% of batch
Ca	23,590	<1	2,172	2,140	27	80.0	99.8	12.22	49,299,716	8908	0.0181	2034	22.8
S	17,770	<1	1,711	1,662	30	51.1	30.9	9.63	nd	7021		973	13.9
Na	2,560	<1	407	378	28	64.2	151	7.13	14,977,060	5198	0.0347	914	17.6
F	3,140	<1	135	129	29	6.80	31.9	7.13	nd	5194		nd	
Al	1,164	<1	63	58	24	4.95	1.79	1.68	49,623,245	1225	0.0025	446	36.4
Cl	11,160	5	1,189	1,162	30	148	116	1.50	nd	1094		140	12.8
Mg	4,240	<1	349	335	27	6.57	5.47	1.36	22,780,688	991	0.0044	257	25.9
Fe	606	<1	24	21	24	<LoD	0.76	1.36	66,279,957	991	0.0015	374	37.8
Si	390	<1	27	25	24	18.4	nd	1.18	182,045,381	860	0.0005	817	95.0
K	788	<1	76	71	26	14.2	17.7	1.02	2,863,742	744	0.0260	82.2	11.1
P	724	<1	74	74	12	0.37	nd	0.20	1,145,187	145	0.0126	19.5	13.5
B	7.72	0.00	2.69	2.61	9	<LoD	0.05	0.18	nd	130		nd	
Mn	144	<1	22	20	22	0.47	0.46	0.107	1,291,854	78.1	0.0060	7.72	9.9
Ti	18.67	<0.001	2.32	2.32	12	0.09	0.05	0.061	11,601,750	44.1	0.0004	38.5	87.2
Zn	53.02	<0.10	4.01	3.58	21	0.17	0.42	0.052	75,643	38.0	0.0502	3.01	7.9
Sr	35.05	0.38	4.63	4.30	14	0.15	0.16	0.029	148,482	21.3	0.0143	4.16	19.6
Cu	95	<1	6	5	22	0.04	0.07	0.027	70,503	19.6	0.0278	1.05	5.3
Sn	0.119	0.008	0.079	0.079	11	nd	nd	0.013	835	9.51	1.1396	0.180	1.9
Se	0.550	<0.025	0.059	0.055	14	nd	0.01	0.010	nd	7.25		1.61	22.1
Ni	3.90	<0.10	0.52	0.50	14	0.05	0.03	0.008	29,038	5.85	0.0202	0.642	11.0
V	0.300	<0.10	0.091	0.089	14	0.01	0.05	0.006	180,735	4.57	0.0025	3.16	69.2
Ba	6.70	<0.10	0.94	0.94	14	0.09	0.05	0.006	66,662	4.16	0.0062	0.600	14.4
Pb	2.07	<0.050	0.14	0.11	16	0.35	0.008	0.003	908	2.53	0.2786	0.110	4.4
Li	1.88	<0.001	0.27	0.22	14	0.10	0.06	0.003	4,438	2.18	0.0491	0.376	17.2
Ce	0.110	<0.010	0.063	0.063	5	0.00	nd	0.003	24,936	2.00	0.0080	0.119	6.0
Y	1.000	0.001	0.035	0.029	6	<LoD	nd	0.003	28,031	1.94	0.0069	0.111	5.7
I						nd	nd	0.002	nd	1.63		0.041	2.5
Nd	0.042	0.008	0.022	0.022	5	nd	nd	0.002	16,309	1.27	0.0078	0.076	6.0
Cr	0.52	<0.050	0.10	0.10	13	0.01	0.02	0.001	34,957	0.94	0.0027	0.289	30.8
Zr	<0.001	<0.001	0.0020	0.0020	6	0.01	nd	0.001	149,009	0.87	0.0006	0.281	32.4
La	0.200	<0.10	0.042	0.041	6	nd	nd	0.001	10,428	0.85	0.0082	0.050	5.9
W	0.0110	0.002	0.0060	0.0060	5	nd	nd	0.0012	178	0.85	0.4785	0.024	2.8
Rb	0.240	<0.015	0.083	0.083	6	0.03	nd	0.0009	6,222	0.67	0.0108	0.076	11.4
Co	1.30	<0.010	0.20	0.19	16	<LoD	0.001	0.0008	27,578	0.60	0.0022	0.146	24.4
Sc						0.02	nd	0.0006	28,441	0.40	0.0014	0.092	22.9
Dy	0.0050	<0.001	0.0020	0.0020	5	nd	nd	0.0005	4,919	0.39	0.0079	0.024	6.2
Gd	0.0070	<0.001	0.0040	0.0040	5	nd	nd	0.0005	4,900	0.36	0.0074	0.021	5.7
Ga	0.033	0.006	0.013	0.013	5	nd	nd	0.0005	13,050	0.36	0.0027	0.197	55.3
Sm	0.0060	<0.001	0.0030	0.0030	5	nd	nd	0.0005	4,489	0.36	0.0080	0.020	5.6
Pr	0.0100	<0.001	0.0050	0.0050	5	nd	nd	0.0004	3,529	0.28	0.0081	0.016	5.7
Nb	<0.001	<0.001	<0.001	<0.001	5	0.05	nd	0.0004	13,864	0.26	0.0019	0.025	9.4
Mo	0.620	<0.040	0.069	0.063	12	0.02	0.02	0.0003	430	0.23	0.0543	0.036	15.5
Ag	1.0790	<0.001	0.0070	0.0010	5	nd	nd	0.0003	nd	0.23		0.012	5.5
Er	0.0020	<0.001	0.0010	0.0010	5	nd	nd	0.0003	2,539	0.19	0.0075	0.013	6.8
As	9.33	<0.10	0.16	0.13	13	0.35	0.01	0.0003	158	0.18	0.1153	0.033	17.9
Yb	<0.001	<0.001	<0.001	<0.001	5	nd	nd	0.0002	2,539	0.15	0.0060	0.010	6.8
Cd	0.337	<0.004	0.057	0.053	15	nd	0.002	0.00018	nd	0.13		0.007	5.1
Eu	<0.001	<0.001	0.0000	0.0000	5	nd	nd	0.0001	1,361	0.10	0.0075	0.007	6.5
Ge	0.0080	<0.001	0.0030	0.0030	5	nd	nd	0.0001	1,140	0.10	0.0090	0.034	32.9
Be	0.0160	<0.001	0.0050	0.0050	6	nd	nd	0.00011	692	0.080	0.0116	0.009	10.6
Hf	0.189	<0.001	0.079	0.079	5	nd	nd	0.00011	2,890	0.08	0.0028	0.009	10.7
Ho	<0.001	<0.001	0.0010	0.0010	5	nd	nd	0.00010	851	0.073	0.0086	0.005	6.2
Ta	0.025	<0.001	0.010	0.010	5	nd	nd	0.00010	704	0.073	0.0104	0.004	5.9
Tb	<0.001	<0.001	0.0010	0.0010	5	nd	nd	0.00010	771	0.073	0.0095	0.004	5.7
Hg	0.0090	<0.001	0.0000	0.0000	11	nd	nd	0.00008	nd	0.058		0.003	5.7
Th	<0.001	<0.001	0.0010	0.0010	5	nd	0.0003	0.00008	898	0.058	0.0065	0.004	6.7
Sb	0.070	<0.010	0.024	0.024	7	0.00	0.001	0.00007	31	0.051	0.1662	0.005	9.8
U	0.0120	<0.001	0.0020	0.0020	9	nd	0.0004	0.00004	5,739	0.029	0.0005	0.002	7.7
Bi	0.150	<0.005	0.014	0.015	11	nd	nd	0.00003	9	0.022	0.2523	0.002	7.3
Lu	<0.001	<0.001	<0.001	<0.001	5	nd	nd	0.00003	387	0.022	0.0057	0.002	7.6
Tl	0.1200	<0.001	0.0060	0.0040	7	nd	nd	0.00003	15	0.022	0.1467	0.002	7.8
Tm	<0.001	<0.001	0.0010	0.0010	5	nd	nd	0.00003	426	0.022	0.0051	0.002	8.1
Cs	0.033	0.001	0.008	0.008	5	0.00	0.0004	0.00002	62	0.015	0.0236	0.002	13.0

ICELAND
Reykjavík
66°N
65°N
64°N
22°W
18°W
14°W
0
25 km
Vatnajökull
64°30’N
Grímsvötn
64°00’N
ISG-5
ISG-6
ISG-8
ISG-7
ISG-4
Kirkjubæjarklaustur
ISG-2
ISG-3
ISG-0
ISG-1
Eyjafjallajökull
Katla
Atlantic Ocean
63°30’N
Vík
19°00’W
18°00’W
17°00’W

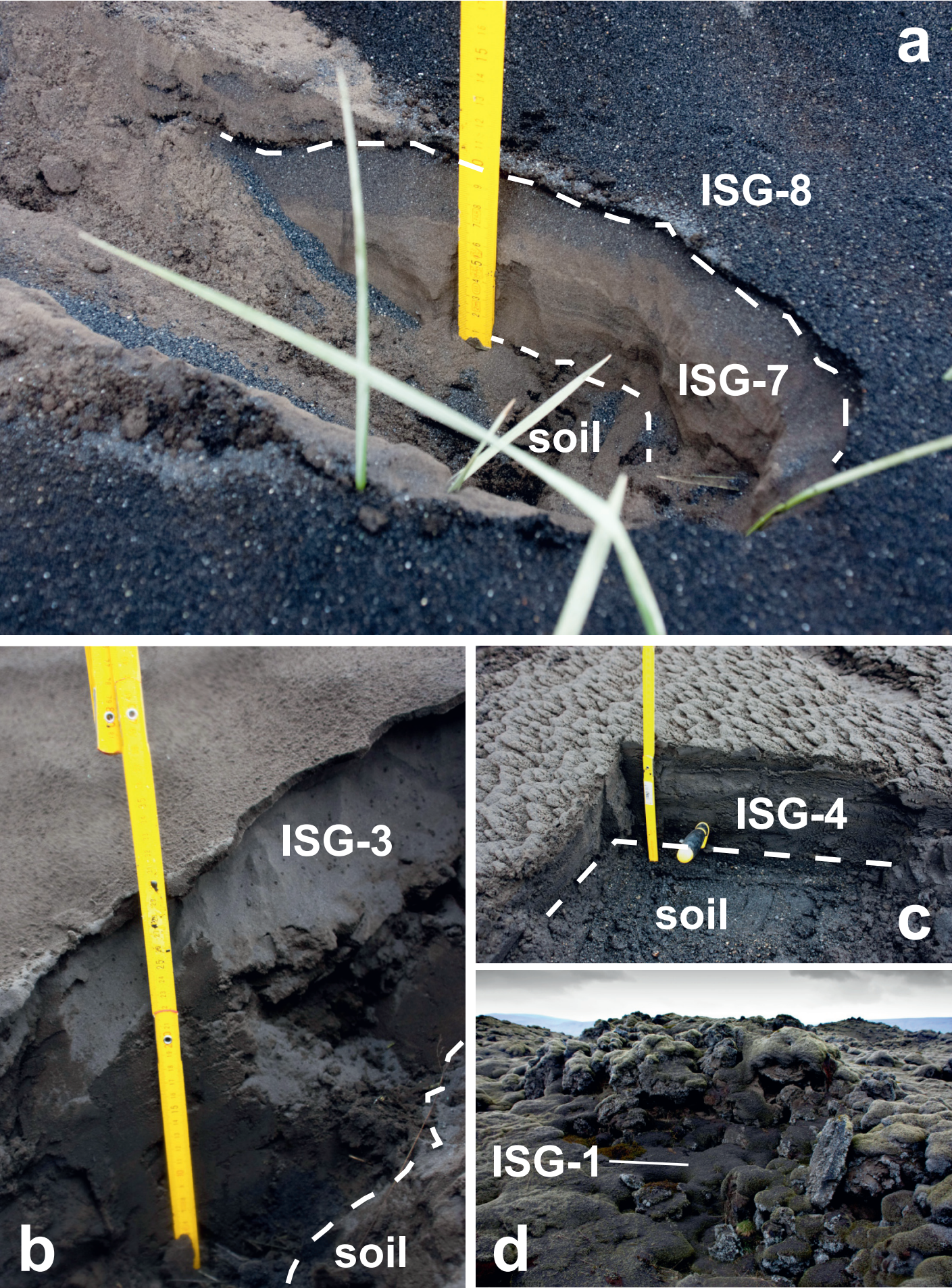
a
ISG-8
ISG-7
soil
b
ISG-3
soil
c
ISG-4
soil
d
ISG-1

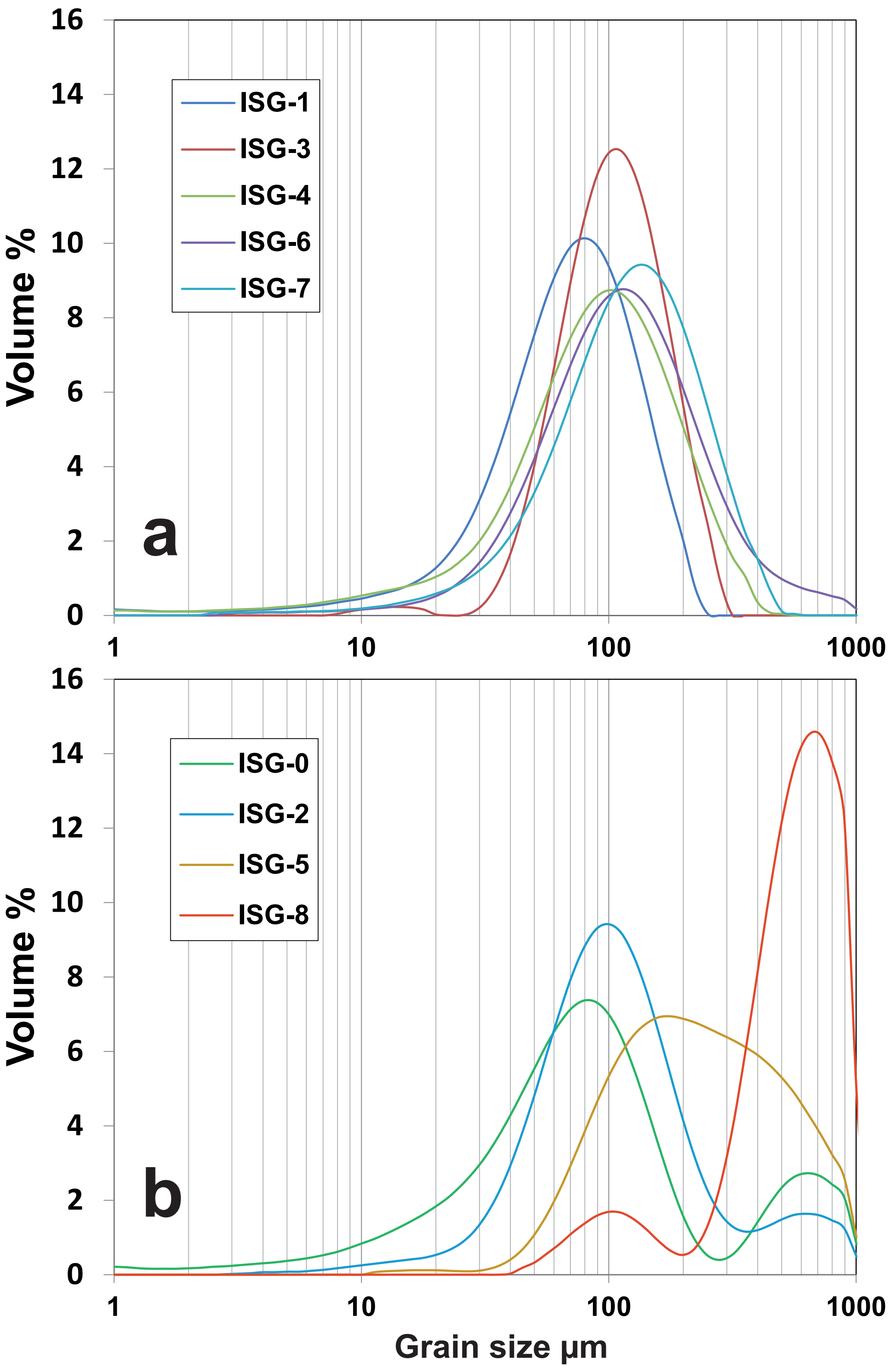
Volume %
16
14
12
10
8
6
4
2
0
ISG-1
ISG-3
ISG-4
ISG-6
ISG-7
a
1
10
100
1000
ISG-0
ISG-2
ISG-5
ISG-8
b
Grain size µm

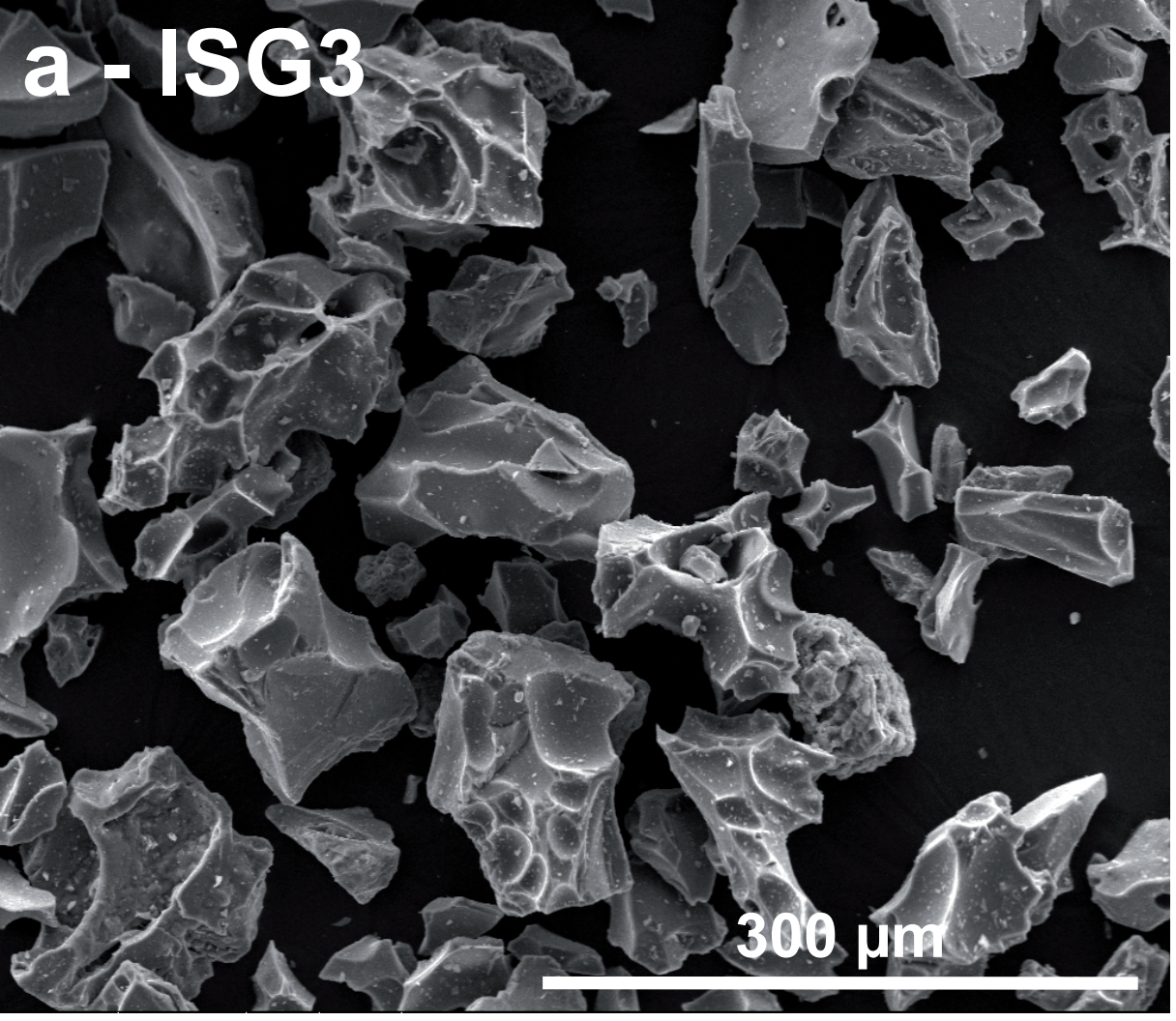
a - ISG3
300 µm

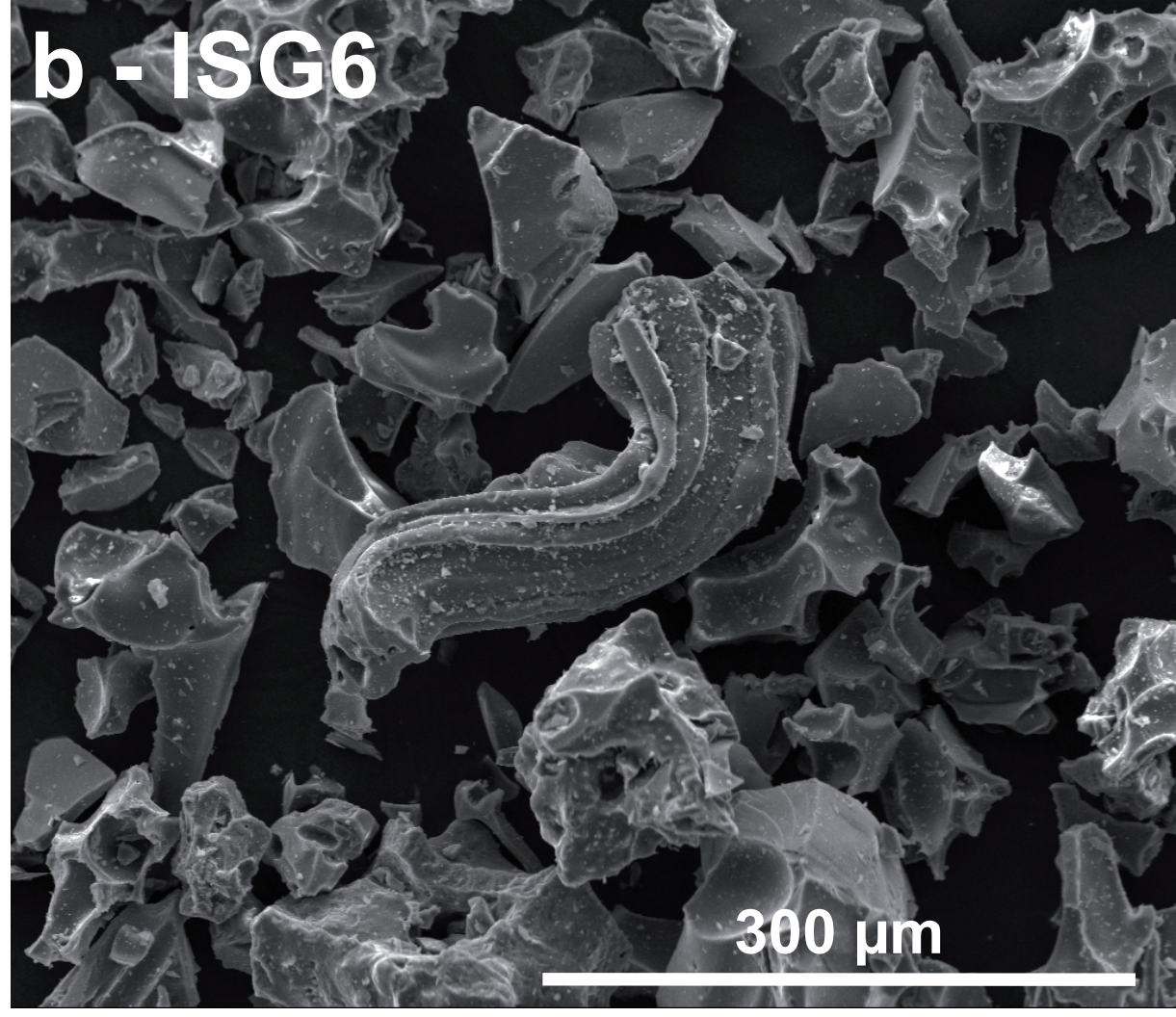
b - ISG6
300 µm

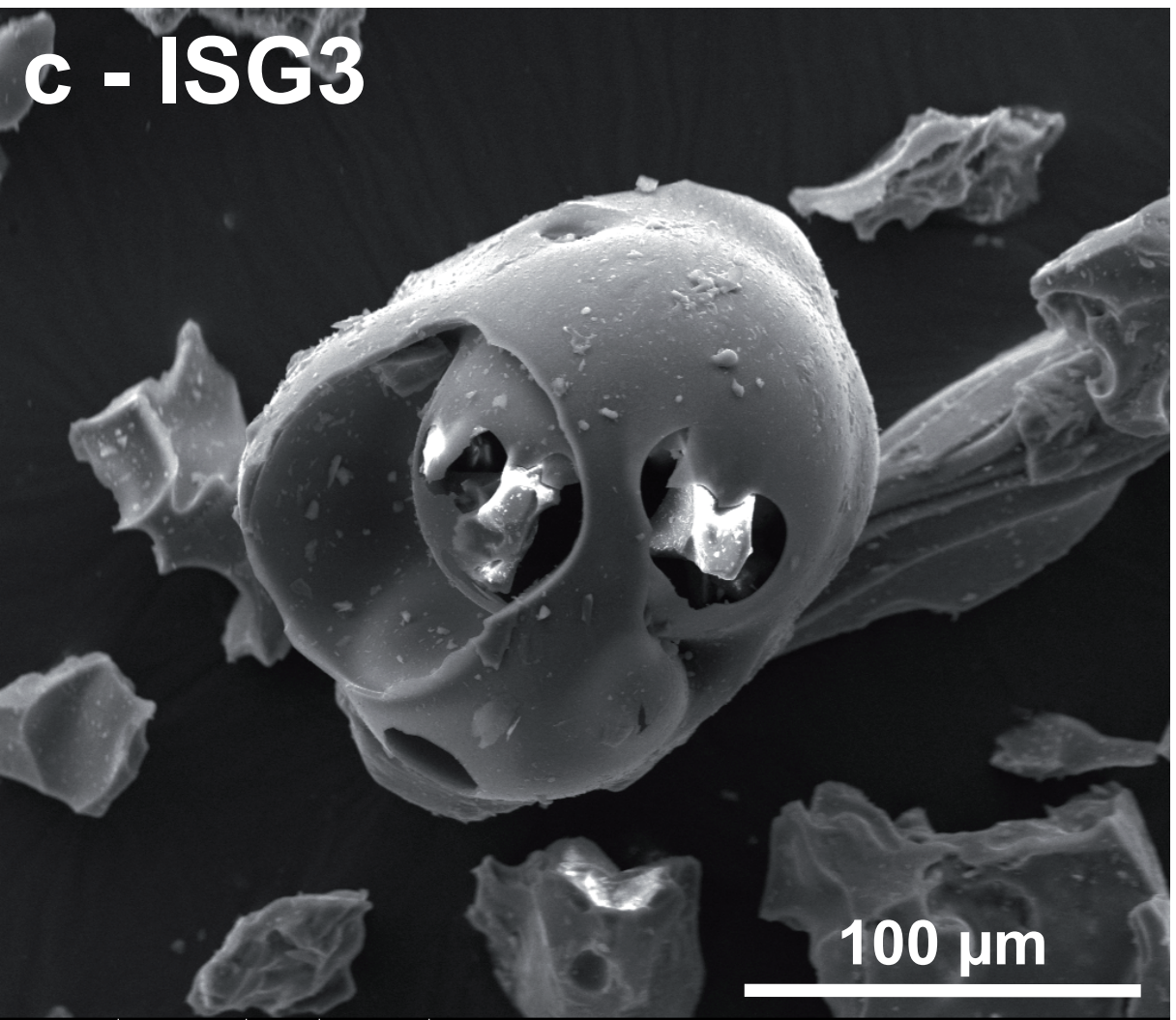
c - ISG3
100 µm

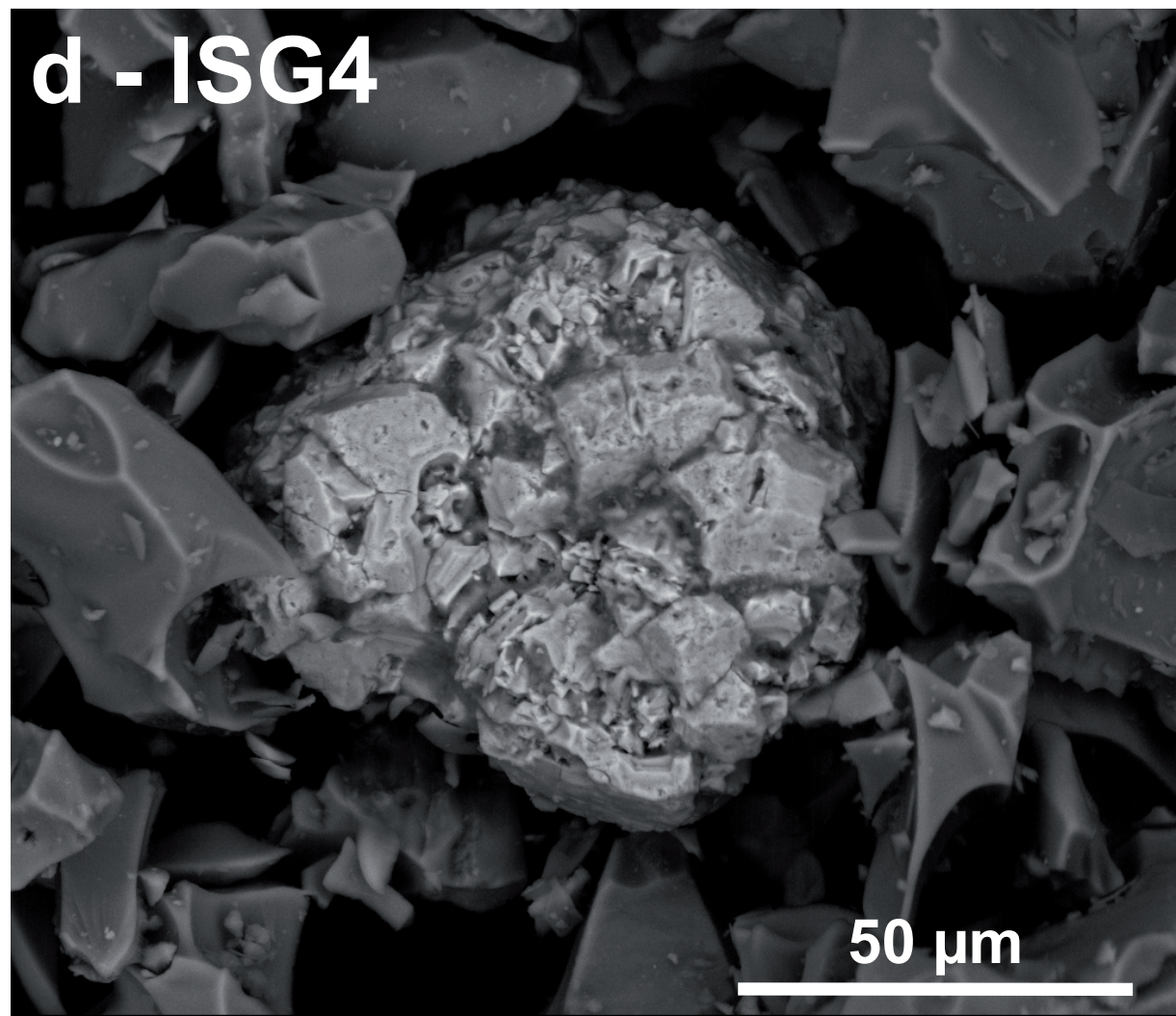
d - ISG4
50 µm

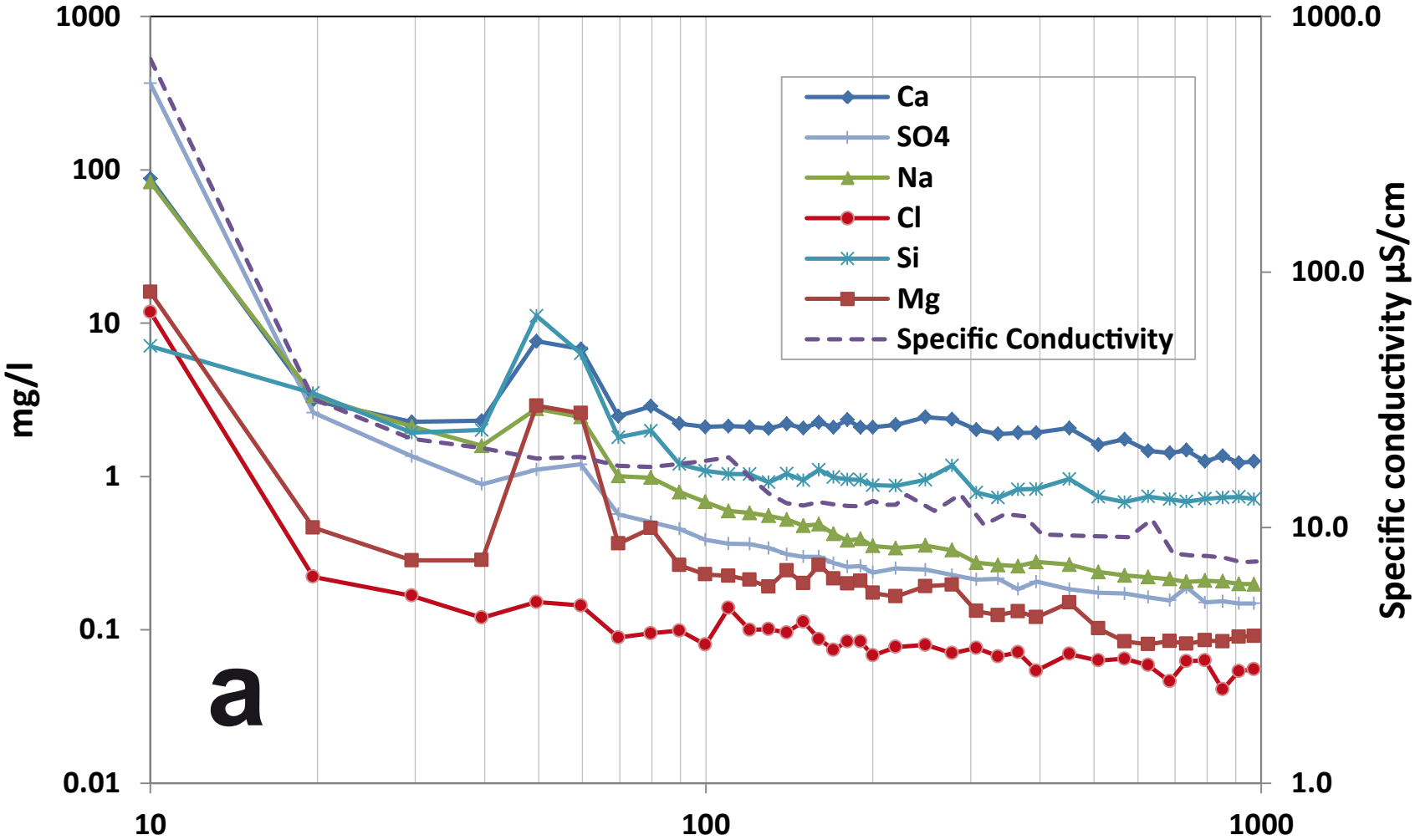
1000
100
10
1
0.1
0.01
mg/l
1000.0
100.0
10.0
1.0
Specific conductivity µS/cm
Ca
SO4
Na
Cl
Si
Mg
Specific Conductivity
a
10
100
1000

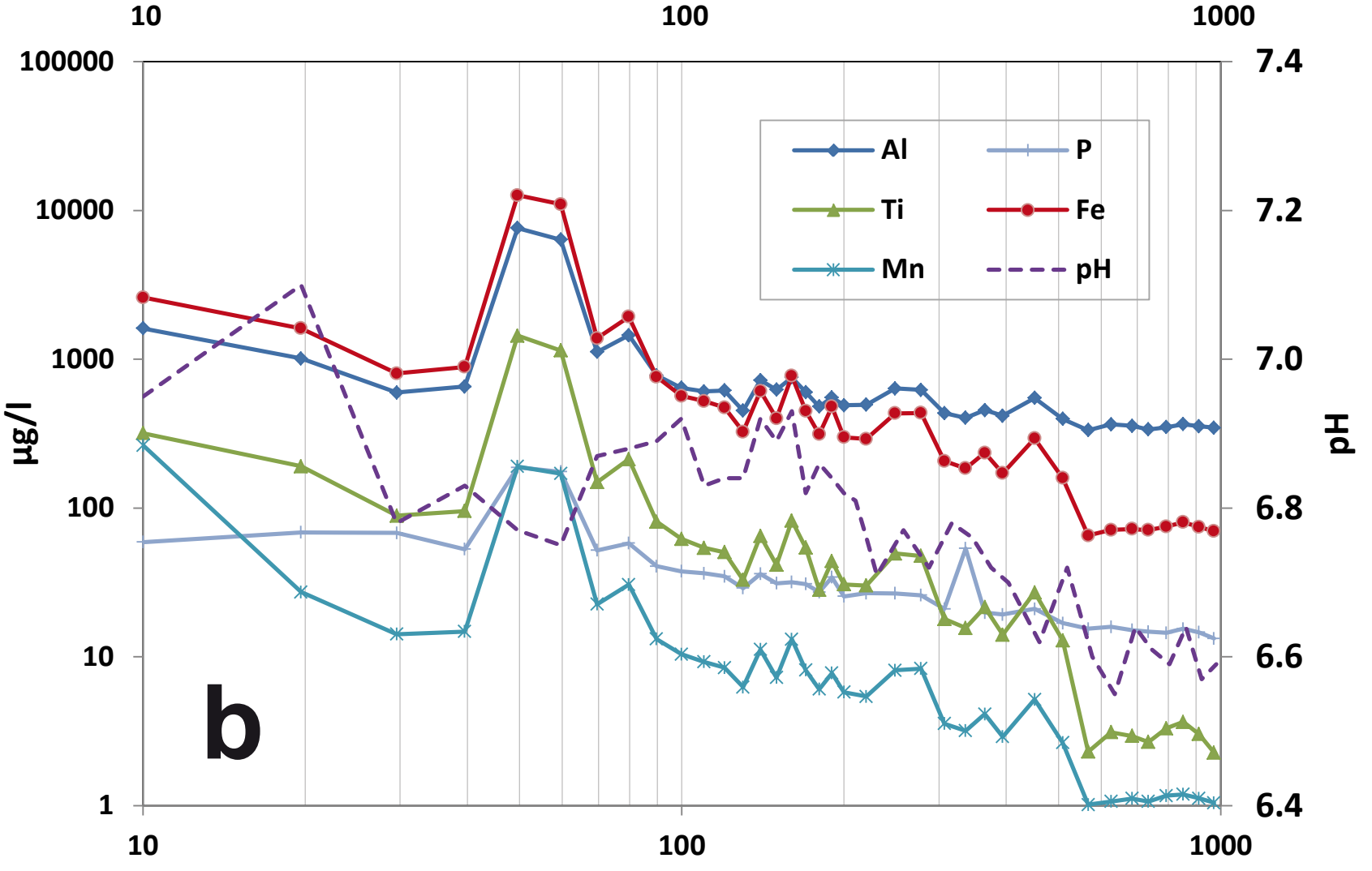
100000
10000
1000
100
10
1
µg/l
7.4
7.2
7.0
6.8
6.6
6.4
pH
Al
P
Ti
Fe
Mn
pH
b
10
100
1000

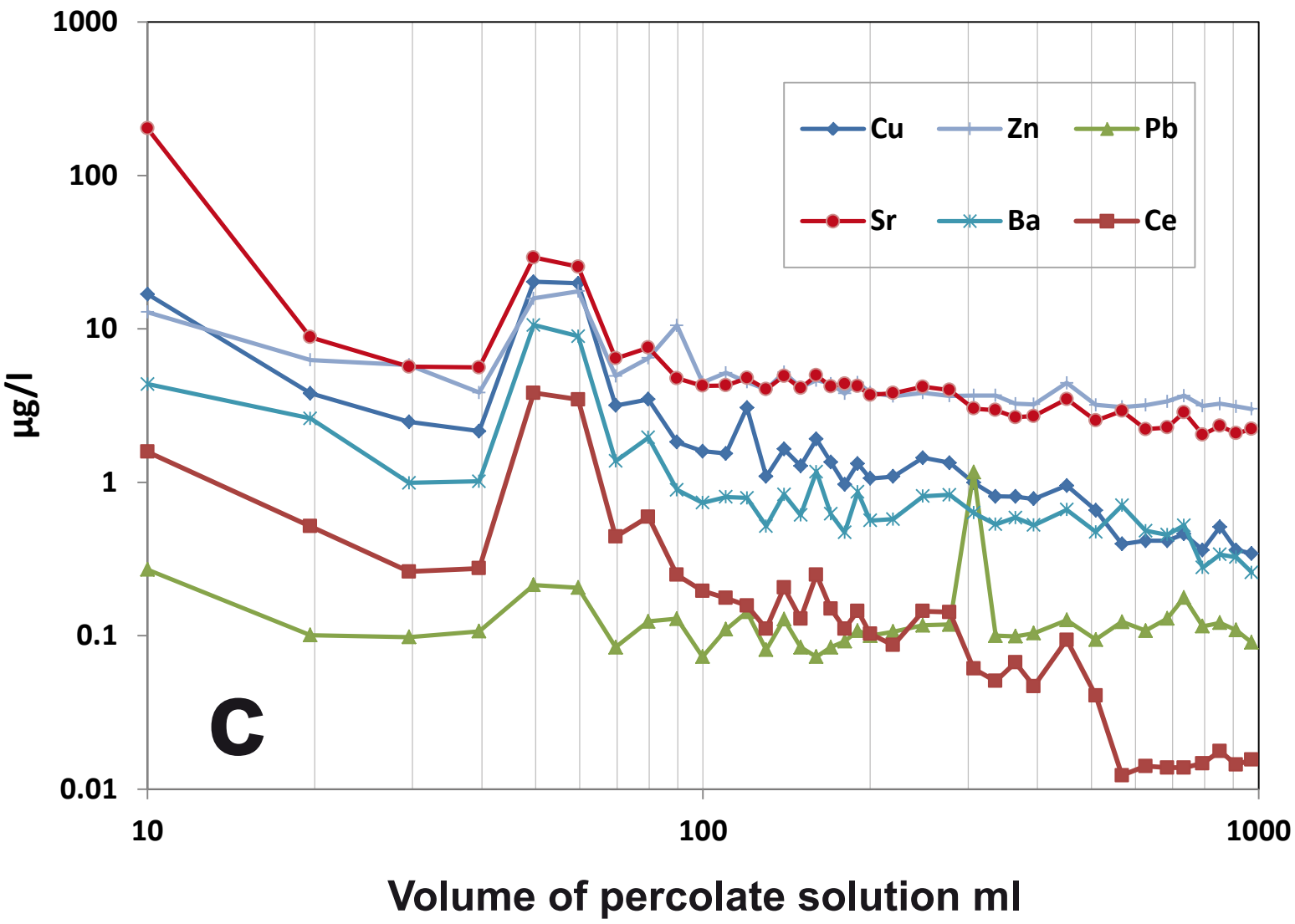
1000
100
10
1
0.1
0.01
µg/l
Cu
Zn
Pb
Sr
Ba
Ce
c
10
100
1000
Volume of percolate solution ml

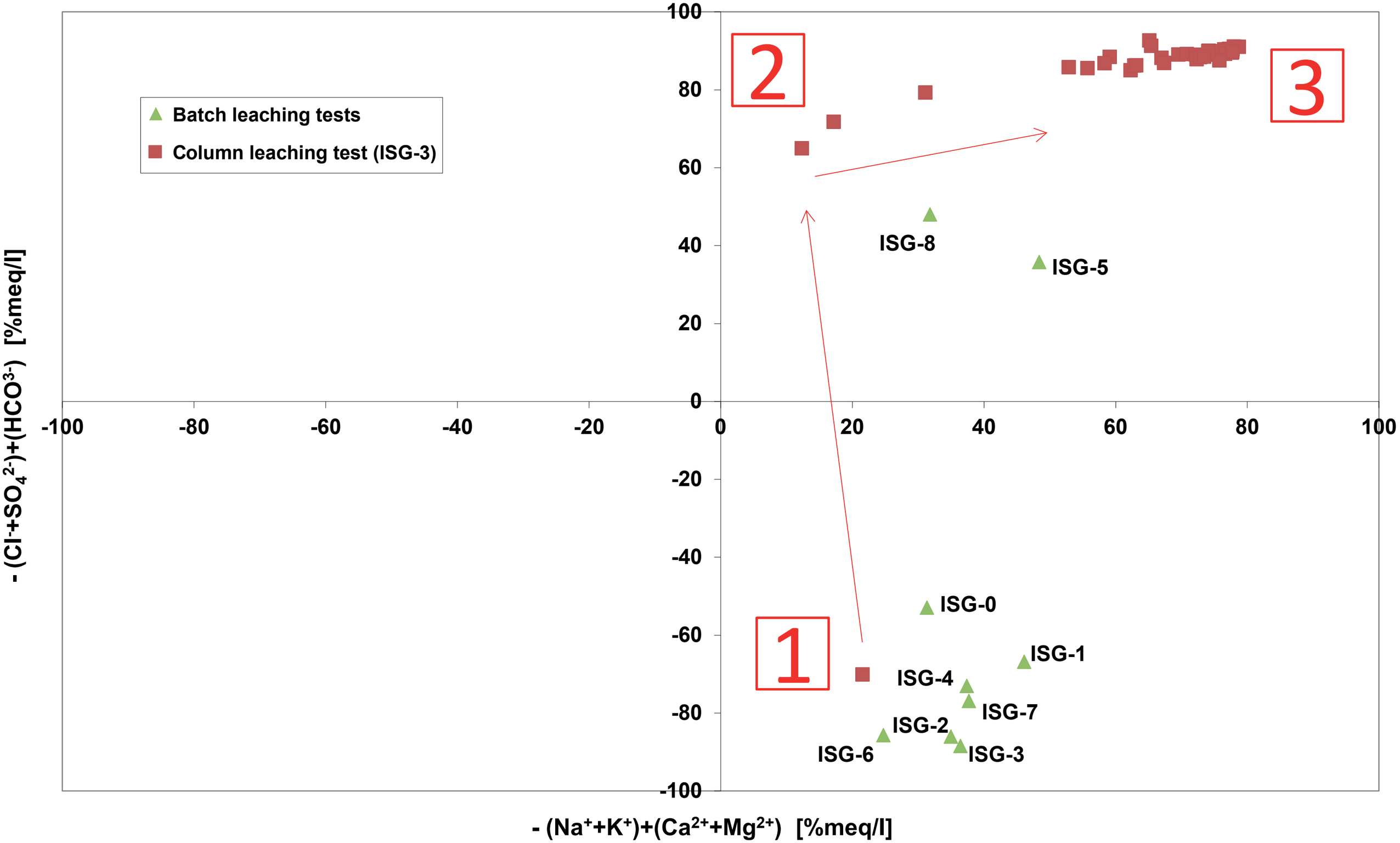
Batch leaching tests
Column leaching test (ISG-3)
2
3
1
ISG-8
ISG-5
ISG-0
ISG-1
ISG-4
ISG-7
ISG-2
ISG-6
ISG-3
100
80
60
40
20
0
-20
-40
-60
-80
-100
-100
-80
-60
-40
-20
0
20
40
60
80
100
- (Cl⁻+SO4 2-)+(HCO3-) [%meq/l]
- (Na⁺+K⁺)+(Ca2⁺+Mg2⁺) [%meq/l]

Supplementary material – Details on analytical methods

Particle size distributions were obtained using a laser diffractometer (Malvern Mastersizer 2000 Hidro-Mu) at the X-ray Diffraction Service of the Institute of Earth Sciences Jaume Almera (ICTJA-CSIC), Spain. It allows the measurement of particles in a range of 0.1 – 1000 μm. For each sample, the results are the average of 3 cycles of 8 s each. The samples were dispersed in Milli-Q plus ultrapure water type (18.2 MΩ/cm). The pump speed was 2500 rpm. A refractive index of 1.52 and absorption of 0.1 were used in the determinations (Blott et al. 2004). The obscuration is 10-20%. Results were then plotted with GRADISTAT (Blott &Pye 2001).

The scanning electron microscope (SEM) analysis was performed with a FEI Quanta 200 ESEM FEG equipped with an Energy Dispersive X-Ray (EDX) system and the GENESIS software for a semi-quantitative chemical analysis (minimum spot size, 5.3 μm; working distance, 9.6 – 10 mm; acceleration voltage, 20 kV). Ash samples were mounted in aluminium stubs and coated with carbon before the study. Analyses were carried out at the Centres Científics i Tecnològics of the Universitat de Barcelona (CCiTUB), Spain.

The mineralogical characterization was determined by X-ray diffraction (XRD) analysis at the X-ray Diffraction Service of the ICTJA-CSIC. The samples were powdered in an agate mortar and the diffractograms were obtained using a Bruker D-5005 instrument (Cu K-α1 radiation, λ = 1.5405 Å, at 40 kV and 40 mA), collecting data between 4 and 60° of 2θ, with a scan step of 0.05° and a

step duration of 3 s. Diffractogram evaluation was carried out using the EVA software.

Concentrations of major and trace elements in bulk ash samples were determined by high resolution-inductively coupled plasma-mass spectrometry (HR-ICP-MS) using a Thermo Scientific Element 2 XR at the labGEOTOP of the ICTJA-CSIC. Analysis was performed on a split (0.1 g) of each sample (9 samples). Before the acid attack, the samples were dried for 24 hours at 40 ºC and then digested with HNO_3:HF:$HClO_4$ (2.5:5.0:2.5 ml, v/v), and doubly evaporated to incipient dryness with the addition of 1 ml of HNO_3; the final solution was made up to 100 ml in a volume flask with Milli-Q plus ultrapure water type (18.2 MΩ/cm). The precision and accuracy of analytical determinations were monitored using reference materials of the Geological Survey of Japan (andesite JA-2 and basalt JB-3) (Imai et al. 1995). Loss on ignition (LOI) was determined by heating 0.5 g of sample at 1000 °C for a minimum of 4 hours. Some LOI values appeared negative due to iron oxidation (Lechler &Desilets 1987).

Blott SJ, Pye K (2001): GRADISTAT: A grain size distribution and statistics package for the analysis of unconsolidated sediments. Earth Surface Processes and Landforms 26, 1237-1248

Blott SJ, Croft DJ, Pye K, Saye SE, Wilson HE (2004): Particle size analysis by laser diffraction. Geological Society, London, Special Publications 232, 63-73

Imai N, Terashima S, Itoh S, Ando A (1995): 1994 compilation values for GSJ reference samples, igneous rock series. Geochemical Journal 29, 91-95

Lechler PJ, Desilets MO (1987): A review of the use of loss on ignition as a measurement of total volatiles in whole-rock analysis. Chemical Geology 63, 341-344